



5-2004

Mechanical Design and Analysis of a Discrete Variable Transmission System for Transmission-Based Actuators

Sriram Sridharan
University of Tennessee - Knoxville

Follow this and additional works at: https://trace.tennessee.edu/utk_gradthes



Part of the [Mechanical Engineering Commons](#)

Recommended Citation

Sridharan, Sriram, "Mechanical Design and Analysis of a Discrete Variable Transmission System for Transmission-Based Actuators. " Master's Thesis, University of Tennessee, 2004.
https://trace.tennessee.edu/utk_gradthes/2205

This Thesis is brought to you for free and open access by the Graduate School at TRACE: Tennessee Research and Creative Exchange. It has been accepted for inclusion in Masters Theses by an authorized administrator of TRACE: Tennessee Research and Creative Exchange. For more information, please contact trace@utk.edu.

To the Graduate Council:

I am submitting herewith a thesis written by Sriram Sridharan entitled "Mechanical Design and Analysis of a Discrete Variable Transmission System for Transmission-Based Actuators." I have examined the final electronic copy of this thesis for form and content and recommend that it be accepted in partial fulfillment of the requirements for the degree of Master of Science, with a major in Mechanical Engineering.

Arnold Lumsdaine, Major Professor

We have read this thesis and recommend its acceptance:

William R. Hamel, Frank H. Speckhart

Accepted for the Council:

Carolyn R. Hodges

Vice Provost and Dean of the Graduate School

(Original signatures are on file with official student records.)

To the Graduate Council:

I am submitting herewith a thesis written by Sriram Sridharan entitled “Mechanical Design and Analysis of a Discrete Variable Transmission System for Transmission-Based Actuators.” I have examined the final electronic copy of this thesis for form and content and recommend that it be accepted in partial fulfillment of the requirements for the degree of Master of Science, with a major in Mechanical Engineering.

Arnold Lumsdaine

Major Professor

We have read this thesis
and recommend its acceptance:

William R. Hamel

Frank H. Speckhart

Accepted for the Council:

Anne Mayhew

Vice Chancellor and
Dean of Graduate Studies

(Original signatures are on file with official student records)

**MECHANICAL DESIGN AND ANALYSIS OF A
DISCRETE VARIABLE TRANSMISSION SYSTEM FOR
TRANSMISSION-BASED ACTUATORS**

A Thesis
Presented for the
Master of Science
Degree
The University of Tennessee, Knoxville

Sriram Sridharan
May 2004

*To
Smt. Mythili Sridharan,
Shri. Sridharan Krishnaswamy
and all my family members*

ACKNOWLEDGEMENTS

Special thanks to my family members who provided me with great encouragement to do this work. I would like to thank all my teachers and friends who have helped me in one way or the other till this point of my life.

I am thankful to my academic advisor Dr. Arnold Lumsdaine, whose technical guidance, suggestions and patience helped in completing this thesis and my master's degree. I am highly grateful to Dr. William R. Hamel for the financial assistance that he provided throughout my master's program and also for his suggestions and ideas as a member of my thesis committee. Thank you Dr. Frank Speckhart for your valuable guidance during this work.

Lastly, I express my sincere thanks to Dr. Spivey Douglas, Dr. Sewoong Kim, Kelley P. Brown, Kalyana Ganti, Renbin Zhou and Ge Zhang who worked with me on the Transmission-Based Actuators and Human Machine Cooperative Telerobotics projects. Thank you all for the support and suggestions that you have provided me.

ABSTRACT

Over the past few years, replacing the hydraulic servo actuators with their electrical counter parts for robotics and remote handling systems has been an active field of research. These systems are of particular interest for tasks involved with the US Department of Energy, where the level of radiation exposure is high and the tasks are highly repetitive. With the hydraulic servo actuators, one is concerned with the issues like the high complexity, cost of the system and the difficulty of maintenance of the system. For high payload operations, the hydraulic systems provide an order of magnitude increase in the power density, which is almost impossible to achieve using the electrical servo actuators. Hence, for the electrical servo actuators to be used for high payload operations, the fundamental issue concerning the power and torque density must be addressed. Previous research conducted on this front suggested the use of a variable speed transmission system to spread the servomotor's torque-speed characteristics across a wider output speed range. This has the effect of allowing smaller high power motors to also deliver high torques at low speeds. By using a variable speed transmission, the motor size can be reduced dramatically while increasing the overall actuator power density in the process. This work goes further into the detailed design of the discrete variable transmission system. A three-stage planetary gear transmission system is considered for the analysis and design.

With the use of the three-stage planetary gear transmission, there are a complex and varied design issues involved. Selecting a configuration for the transmission is the first question to be answered. With the given configuration, and the ratios required the individual gears have to be sized accordingly. Other design elements involve the design of the shafting, achieving the desired configuration, bearings, housing and the design of a gear shifting mechanism. A detailed kinematic and dynamic analysis of the entire gear system is required for the design of the various components mentioned above. Analytical results are presented along with a computer-aided analysis of the work using the Pro-Engineer design and analysis software. Future work on this will be to turn this into a commercially available system, which comes down to optimizing the current design. Possibilities of optimization for the current design will be identified. A discussion on the prototype evaluation of the transmission system along with a sample test result is presented.

TABLE OF CONTENTS

1.Introduction	1
1.1 Background Information.....	1
1.2 Comparison of Robotic Actuators	4
1.3 The Concept of Transmission Based Actuators (TBA)	5
1.4 Scope of this Work.....	8
2.Concept Of Discrete Variable Transmission	9
2.1 Baseline Requirements.....	9
2.2 Gear Trains.....	11
2.3 Configuration for the DVT	16
2.4 Breaking Down the Design into Components	20
2.5 Summary.....	22
3.Analysis of the DVT System	23
3.1 Speed Equations.....	23
3.2 Torque Equations.....	27
3.3 Summary.....	37
4.Detailed Design of the DVT	38
4.1 Sizing of the Gears.....	38
4.2 Design of Planet Carriers	44
4.2.1 The Final Carrier.....	45
4.2.2 Tolerances and Fits	51

4.3 Bearing Selection	55
4.4 DVT Housing.....	58
4.5 Brake Mechanism Design	61
4.6 Summary	67
5.Virtual Model of the DVT in Pro/Engineer	68
5.1 Introduction.....	68
5.2 CAD Model Representation of DVT Components.....	70
5.3 Pro-Mechanica Motion Analysis	74
5.3.1 Single-stage Planetary Gear Train	76
5.3.2 Three-stage Planetary Gear Train	80
5.4 Gear Tooth Stress Analysis.....	84
5.4.1 Gear Tooth Failure Modes.....	86
5.4.2 Finite Element Modeling of the Gear Teeth	87
5.5 Summary	90
6.Conclusions and Future Research	91
6.1 Conclusions.....	91
6.2 Future Work	94
Bibliography.....	97
Appendix	100
Vita.....	115

LIST OF FIGURES

Figure 1 – Schilling Titan 2 Manipulator	2
Figure 2 – Torque-Speed Relations	7
Figure 3 – Exploded View of a Single Planetary Gear Train	15
Figure 4 – Carrier-Carrier Configuration.....	17
Figure 5 – Carrier-Ring Configuration	19
Figure 6 – Exploded View of a Carrier – Ring Configuration	19
Figure 7 – Free Body Diagram of a Single Planetary Gear Train	28
Figure 8 – Diagram of Internal Torques for a Three-Stage Planetary Gear Train	35
Figure 9 – The Finished Input Shaft	42
Figure 10 – Relative Hardness Levels for Steel and Iron Gears.....	43
Figure 11 – DVT Carriers.....	46
Figure 12 – Final Carrier Dimensions	48
Figure 13 – Spline Selection.....	49
Figure 14 – Snap Rings.....	50
Figure 15 – Shaft and Housing Shoulder Tolerances	51
Figure 16 – Snap Ring Tolerance Values	52
Figure 17 – Ranges of Shaft and Housing Fits	53
Figure 18 – Shaft Tolerance Values Based on the Grade of Fit	55
Figure 19 – Single Row Deep Groove Ball Bearing.....	56
Figure 20 – DVT Housing 3D Model and Dimensions	60
Figure 21 – Conceptual Design of the Brake Mechanism	62
Figure 22 – DVT Brake Mechanism.....	63
Figure 23 – L-Bracket and the Complete Brake Mechanism	64
Figure 24 – Band Link Finite Element Model	65
Figure 25 – Stress Results for the Band Link	66
Figure 26 – Pro-Engineer Model of the Three-Stage DVT	73
Figure 27 – Pro-Mechanica Results for a Single Planetary Gear Train.....	77
Figure 28 – Arm Configuration for Prototype Evaluation.....	81
Figure 29 – Position, Velocity and Acceleration Profiles.....	82
Figure 30 – Pro-Mechanica Results for a Three-Stage Planetary.....	85
Figure 31 – Loads and Constraints on a Single Spur Gear Tooth	88
Figure 32 – Gear Teeth Stress Results.....	89
Figure 33 – DVT Components and Assembly	92
Figure 34 – DVT Test Setup.....	93
Figure 35 – DVT Sample Test Result.....	94
Figure 36 – Two-Stage DVT	95

GLOSSARY

Symbol	Explanation
ω_C	Angular velocity of the carrier
ω_R	Angular velocity of the ring gear
ω_S	Angular velocity of the sun gear
ω_P	Angular velocity of the planet
T_S	Number of teeth on the sun gear
T_P	Number of teeth on the planet gear
T_R	Number of teeth on the ring gear
τ_S	Torque on the sun gear
τ_L	Load torque
τ_B	Brake torque
τ_{RR}	Reaction torque of the ring gear
τ_{RC}	Reaction torque of the carrier
F_{PS}	Contact force at the sun-planet mesh
F_{PR}	Contact force at the planet-ring mesh
F_{CP}	Force that the carrier puts on the planet
r_{TH}	Thickness of the ring gear
r_S	Radius of the sun gear
r_R	Radius of the ring gear
J_S	Inertia of the sun gear
J_P	Inertia of the planet
J_C	Inertia of the carrier
m_P	Mass of the planet

$\dot{\omega}_S$	Acceleration of the sun gear
$\dot{\omega}_R$	Acceleration of the ring gear
J_R	Inertia of the ring gear
D	Diameter of the solid shaft
T	Torque carried by the shaft
N_{FS}	Factor of Safety
S_{YP}	Yield strength of the material
D_{re}	Minor diameter of the external spline
L	Length of the spline
D_P	Pitch diameter of the spline
R_D	Diameter ratio of the shaft
D^l	Operating pitch diameter of the gear
M_p	Mass of the payload
M_a	Mass of the arm
g	Acceleration due to gravity
m_g	Gear ratio
θ	Position of the arm
t	Time
$\ddot{\theta}$	Acceleration of the arm
r_P	Radius of the planet gear

1.1 Background Information

Robotics is the science and art of performing tasks by means of an automatic apparatus or device, functions ordinarily ascribed to human beings, or operating with what appears to be almost human intelligence[1]. The automatic apparatus or device used to perform the task is called a *robot*. Basically a robot may consist of a mechanical device such as a wheeled platform, a manipulator arm or other construction devices capable of interacting with the environment, sensors on or around the device that are capable of sensing the environment to give useful feedback information and systems that process the sensory input the context of the device's current situation and instruct the device to perform actions in response to the situation. Designing, building, programming and testing a robot is a combination of physics, mechanical engineering, electrical engineering, structural engineering, mathematics and computing. In some cases biology, medicine, chemistry might also be involved.

A *manipulator arm* is a system of structural members connected together by joints. The typical joints are prismatic and revolute type. Manipulator arms imitate the human arm in appearance and functionality. They are comprised of shoulder, elbow and wrist and they have a pitch, roll and yaw motion. The

shoulder is the highest load-carrying joint of the manipulator arm and also it offers the widest range of motion possible. It provides the overall orientation of the manipulator. The elbow provides the radial extension or the reach and the wrist provides the final orientation of the end effectors[2]. The envelope on the 3D space that the manipulator can reach is referred to as the workspace of the manipulator. Figure 1 shows the configuration of TITAN3 manipulator. Each of the joints in the manipulator receives power for their motion from the actuators. Actuators may be electrical, hydraulic or pneumatic type. There is a great deal of research effort devoted to the developing more efficient and reliable robot actuators[3][4]. A detailed discussion of the various kinds of robot actuators is made in the section 1.2.

Robots are used in diverse applications and hence the design and functionality varies with each task. Robots have several advantages over humans, which make them extremely suitable in industrial environments, hazardous mines and situations where the work is monotonous. Moreover they have the ability to consistently produce high quality products and to precisely perform tasks. Some of the applications of robots include,

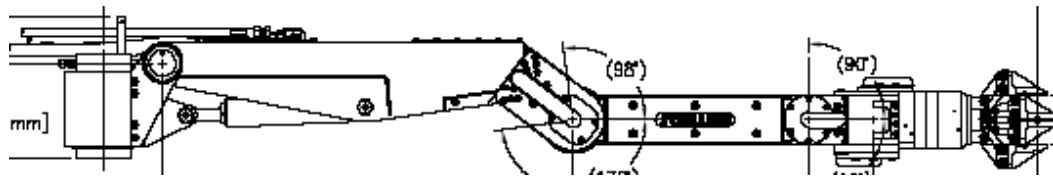


Figure 1 – Schilling Titan 3 Manipulator

- ✓ Space exploration, where a human operator on the earth can control partially autonomous manipulators on the moon or other distant planets.
- ✓ Use of robotic manipulators by the U.S Department of Energy for decontamination and dismantling operations of nuclear wastes or toxic weaponry where human interaction is not possible.
- ✓ Virtual reality systems that are used to train and educate people. The main component of this system is the haptic interface that allows the user to feel the environment and to exert forces on it.
- ✓ Medical applications such as the robot assisted surgery, where a surgeon directs the robot to make controlled high precision incisions with very high accuracy.
- ✓ Industrial applications for automating production lines. Examples are welding, spray painting and other repeated operations performed by robots.

Robotics is still a growing field of engineering and hence a huge amount of research is dedicated to several areas of robotics. Development of good communication between the sensors, computers and the robots is one of the significant problems in robotics[2]. Lack of common communication standards creates real problems when integrating robots and sensors into a work cell. Development of reliable and compact actuators that improves the performance of the robot manipulators is another area of active research[3][5]. Many problems in kinematics, dynamics of robot motion, perception of the environment from

sensory information, hybrid control of manipulators, navigation in unstructured environments and control of high flexibility robot links are yet to be solved[6]. In the recent years Haptics, which deals with providing the operator with force feedback from the environment, has become an active area of research[7].

1.2 Comparison of Robotic Actuators

Actuators are the source of power for a robot. Typically they are linear or rotary actuators and they may be electrically, hydraulically or pneumatically actuated. Electrical actuators use the electric motor as a source of power. Power is transmitted to the joint of the robot through the transmission elements like belts and gears. Hydraulic actuators convert the energy supplied by the pressurized fluid into rotation or extension. The hydraulic fluid flowing through the actuator is generally controlled by electro magnetically actuated servo valves or by pumps. Pneumatic actuators use compressed gas as the source of power. The most common application of pneumatic actuators is the opening and closing of the grippers. Much research is focused on developing modern piezo-electric actuators and shape memory alloys as actuators[8][9]. The type of actuator used depends on the application for which it is required and the environmental conditions. So each type of actuator has its own advantages and disadvantages.

Designing actuators that are reliable and compact is essential in robotic applications. Power density (power to mass ratio) and torque density (torque to mass ratio) are important criteria in evaluating a robotic actuator. Hydraulic

actuators have a very high power and torque density, meaning they can produce very high power and torque with a low mass. But they are mechanically more complex and require periodic maintenance. Other problems with employing a hydraulic actuator is that they are expensive, they need a remote power source that uses large floor space and they have frequent leakage of the oil pipes. These disadvantages are overcome to a great extent with electrical actuators. Moreover, electrical actuators are fast and accurate, relatively inexpensive and have the possibility to apply sophisticated control techniques to motion. One major disadvantage of electric motors is that they have a very low power and torque density. So to produce the torques required for high payload operations, the size and mass of the electric motors become very high. A detailed discussion on this topic can be found in [10]. Therefore electrical actuators are normally used with some type of speed reducers to amplify the torque of the electric motor. Even the speed reducer unit becomes huge to produce high torques with a reasonably small motor. Hence electric actuators cannot produce the torques on the level of what is achieved with hydraulics, in a given space. Because of this reason, systems in the high payload regions are often implemented using electro hydraulic actuators[11].

1.3 The Concept of Transmission Based Actuators (TBA)

This section introduces the concept of the “transmission based actuators” for robot manipulators, originally introduced by Dr. Bill Hamel and T.C Widner.

The previous section addressed the issue of power and torque density of actuators. The main idea behind the TBA concept is the introduction of a variable speed transmission with the electric motors. With this, the torque-speed characteristics of the motor are spread over a wider output speed and torque range[11]. This allows the use of small high power motors to provide high torques at low speeds, thus extending the use of electric motors for high payload conditions such as the remote handling operations with the U.S Department of Energy.

The motor – transmission combination can be selected based on the load requirements and the gear ratios can be optimized accordingly. When high torques are needed at the joint, for example the case when the payload is to be moved from rest where the inertial effects of the arm and the payload are high, the transmission can be operated at its first gear thus delivering high torques. When the torque requirement goes down torque can be traded for speed, unlike fixed gear reductions, which can serve only one purpose - either the torque or the speed requirement. A graphical representation of this is shown in the Figure 2. The first graph shows the changing gear ratios with time. The second plot is the representation of the torque-speed characteristics of the joint in each gear. The first gear is engaged to move the joint from rest or other similar loading conditions. The lower gears are used when the torque requirement goes down, offering a speed increase. A motor-transmission combination can be utilized at each joint (commonly known as the distributed actuation) according to the load

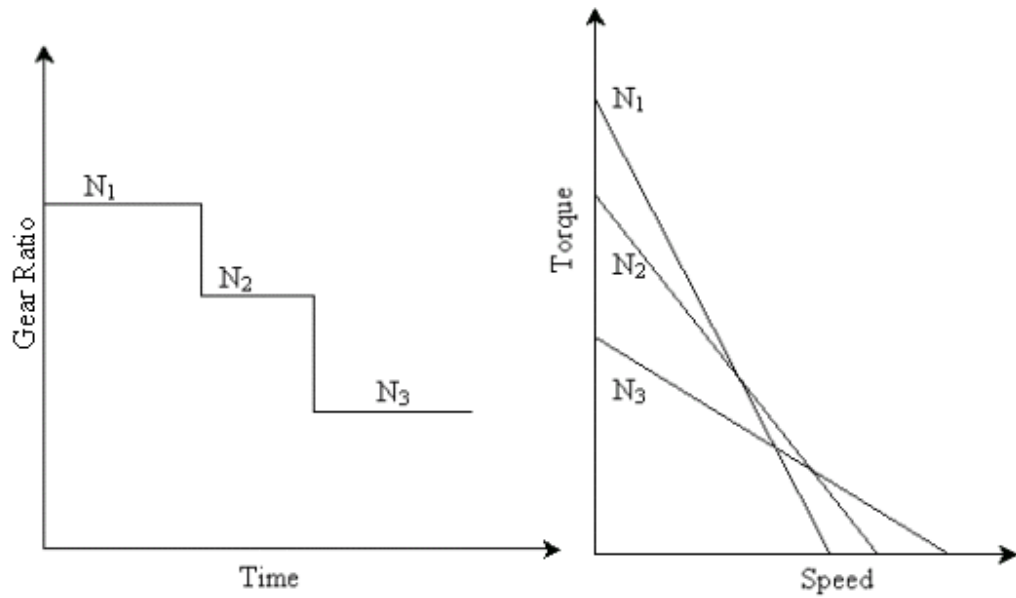


Figure 2 – Torque-Speed Relations

requirements of the joint, thus eliminating the need for transmission elements to transmit the power from the actuator to the corresponding joints, as in the centralized actuation.

The TBA can be thought of as several single stage transmission units built into a single unit. Hence different types of loading conditions can be accommodated which makes the system robust. The advantages of the system are multiplied when it is allowed to change gear ratios during the joint motions. This concept can be considered analogous to an automobile transmission.

1.4 Scope of this Work

Previous work by Dr. Bill Hamel and T.C Widner[11] was a pioneering effort into introducing the concept of transmission-based actuators. Feasibility study of TBA using the Advanced Servo Manipulator as the baseline was performed. Centralized vs. Distributed actuation was studied and the various control aspects of the TBA were identified. A Discrete Variable Transmission (DVT) and a Continuous Variable Transmission (CVT) were proposed for TBA. Preliminary design alternatives for the DVT and CVT were examined. This work is primarily focused on developing the prototype for the TBA. The design of the discrete variable transmission is considered in this work. In a general sense, this thesis work will be focused on the conceptual design, detailed design and the analysis of the DVT system. The design of the DVT system will begin by defining the design requirements and finish with an assembled transmission prototype unit ready for the testing. Some of the specific tasks will be the detailed design of the gear train components, finite element model of the brake linkages, a Pro/E dynamic model of the transmission system and finite element model of the gear teeth based on the forces obtained from the Pro/Mechanica motion results. Finally an effort is made to provide information for optimization of the system that will lead the way to future research. The ultimate goal is to optimize the DVT system, so that it can replace the hydraulic manipulators for almost any kind of loading condition.

Chapter 2

Concept Of Discrete Variable Transmission

The first chapter was an introduction to the concept of transmission-based actuators, and a discussion on the types of TBA was presented. This chapter talks about the DVT in more detail. Requirements for the detailed design and conceptual design of the DVT, components of the DVT and the issues involved in designing the prototype will be presented.

2.1 Baseline Requirements

The concept of transmission-based actuators was introduced in the chapter one and the main idea behind this research was to develop a TBA that could match the performance of a hydraulic actuator for high payload conditions. The schilling TITAN 3 manipulator, used in the decontamination and dismantling operations by the DOE is used as the baseline for the performance evaluation of TBA. As described earlier, since the shoulder is the highest load-carrying joint, the design was set to meet the load requirements for this joint. The size requirement on the TBA is yet another issue to be considered. The entire system should be designed to fit in an enclosure 5”x4”x7”, which conforms to the volumetric space of TITAN 3 manipulator. Table 2.1 presents the specifications of the TITAN 3 hydraulic system.

Table 2.1 – TBA Baseline Requirements

	Metric	English
Maximum Reach	1915 mm	75.4 in
Maximum payload at full extension	113 kg	250 lbf
Weight	102 kg	225 lbf
Approximate C.G location	1000mm	39.37 in
Maximum angular velocity – No load	42 deg/sec (7rpm)	42 deg/sec (7rpm)
Maximum angular velocity – Full load	20 deg/sec (3 rpm)	20 deg/sec (3 rpm)
Maximum angular velocity – Half load	30 deg/sec (5 rpm)	30 deg/sec (5 rpm)

Based on the simulation results obtained by Dr. Sewoong Kim and Renbin Zhou, it was determined that the maximum total torque that must be generated by the TBA system under the most extreme circumstances of full static and dynamic loading should be 3481.9 N-m. The power requirement, as estimated from the product of the torque and rotational velocity, was shown to be 1248.1 watts under full loading conditions and 1215.4 watts under half load. Thus the performance requirements for the TBA are[‡],

- ✓ The arm weighing 102kg, with the center of gravity at 1m from the rotational axis, having a maximum load of 113kg.
- ✓ The arm must be capable of accelerating from rest to a maximum rotational velocity of 7 rpm under no load conditions in 0.5sec and

[‡] Obtained from a Robotics Laboratory Internal Document

maintain this speed. Full load maximum velocity is 3.33 rpm and must be achieved in 0.5 sec also.

- ✓ A torque requirement of 3500 N-m will be used as the goal in the design process.
- ✓ The system must sustain at least 1250 watts across all speeds, loads and orientations. Based on the efficiency of the transmission system, a motor with a rated power of 2000 watts was suggested.
- ✓ A TBA with ratios of 3:1, 4:1 and 7:1 was recommended to achieve the above goals with a motor having a rated speed of 5000 rpm, a continuous stall torque of 4.74 N-m and a power of 2Kw.

A gear reduction of 5-10:1 was assumed at the arm, which will be a part of the actual manipulator design itself. So a TBA with the above-specified ratios along with a final gear reduction of 20:1 was required to be built. With all the specifications established for the TBA design, the following sections will describe the conceptual design of the DVT system.

2.2 Gear Trains

A gear train is the arrangement of the individual gears viz., spur, helical, bevel etc., in a specific arrangement to transmit motion or power from one shaft to another. Table 2.2 shows the arrangement of gears in some of the most common gear trains. The configuration of the gear train used depends on the velocity ratio required and the relative position of the axes of the shafts. Some

Table 2.2 – Types of Gear Trains

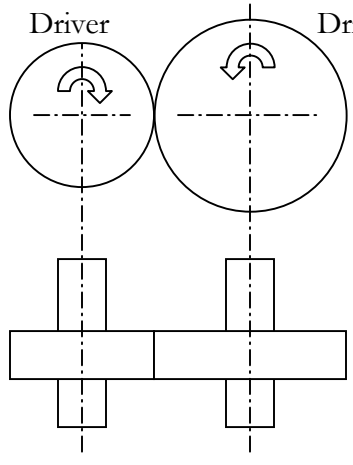
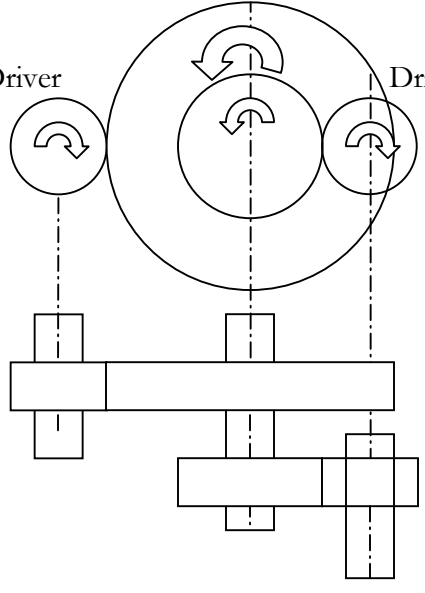
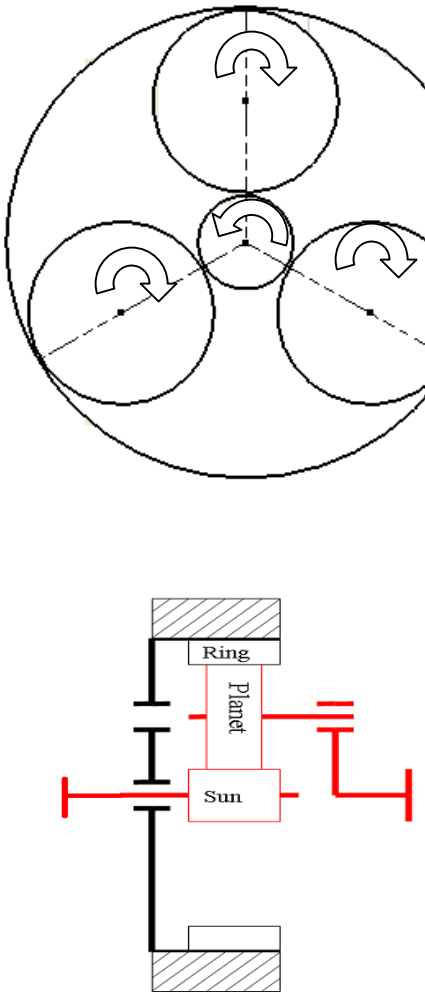
Gear Train	Arrangement of Gears	Description
<p>Simple Gear Train</p>		<p>Gear trains with just one gear mounted on each shaft. Used when the center distance between the gears is small. Idler gears are used if they operate at large center distances.</p>
<p>Compound Gear Train</p>		<p>Gear trains with more than one gear on each shaft. Used when the gear center distances are too large and also when large reductions are required in the order of 7:1 or higher.</p>

Table 2.2 Continued

Gear Train	Arrangement of Gears	Description
<p>Planetary Gear Train</p>		<p>Gear trains with concentric arrangement of gears. Used when very high reductions are required within a limited amount of space. Also known as epicyclic gear trains. Used in most of the automobile transmission systems.</p>

examples are Simple, Compound, Reverted and Planetary gear train.

The type of gear train used for the TBA is the planetary arrangement of gears. A simple planetary gear train consists of three gears viz., the sun, planet and the ring gear. Figure 3 shows an exploded view of the planetary gear train arrangement. The sun and ring gears rotate about the same axis. The planets are assembled in the carrier, which also rotates about the same axis as the sun and ring gears. The planet gears mesh with both the sun and the ring gears and they, apart from rotating about their own axis also rotate about the axis of the sun gear. The number of planets used depends on the loading conditions and a greater number of planets are used to distribute the load among them. All the planets are equally spaced and a minimum of two planets is required for the gear train.

Planetary gear trains are two degree of freedom systems. This means that it requires at least two inputs to get a determined output from the system. Typically the sun gear is the input and the carrier shaft provides the output. Fixing the ring gear provides the second input to the system. This kind of arrangement provides a speed reduction and a torque increase. In fixed reduction drives that provide only one reduction, the ring gear is built into the housing supporting the gear train. However there are several configurations in which the gears can be arranged and each of them provide a speed increase, decrease, a neutral or a direct drive depending on which member of the train is locked. For example a speed increase can be achieved when the sun gear is held stationary, the input being the planet carrier and the output being the ring gear.

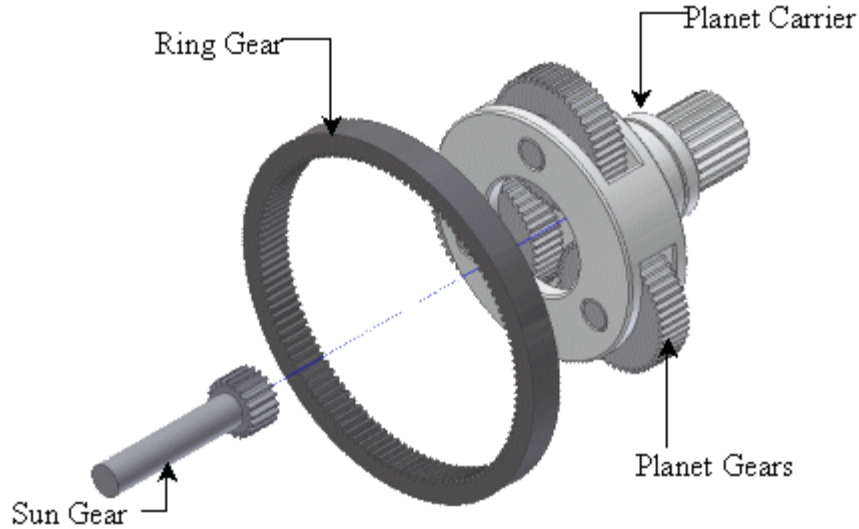


Figure 3 – Exploded View of a Single Planetary Gear Train

The number of times a planet pinion rotates on its shaft while making one complete revolution around the sun gear depends on the ratio between the sun gear and the planet gear. When all the members are free to rotate, no power can be transmitted through the system, as it is under determined. This condition provides the transmission with a neutral position. In the case where any two members of the gear train are locked, the entire system is locked and both the input and output shaft rotate at the same speed providing a 1:1 gear ratio.

Planetary gear trains offer several advantages over the other gear trains. They can offer a very large gear reduction in a very small space because of the concentric arrangement of the gears. Also, they offer several configurations with the same gears. These advantages make them extremely suitable for the transmission-based actuators.

2.3 Configuration for the DVT

Selecting the configuration for the DVT was an important design decision. Recall that the TBA is required to spread the torque-speed characteristics of the motor to a wider output torque and speed range. To realize this, a three-speed transmission with three interconnected planetary gear trains was designed. Even with a two stage planetary gear train, the three speed ratios could be achieved (by using a clutching mechanism) but for the sake of simplicity of prototype, a three stage DVT was proposed. Gear shifting is made possible by stopping the ring gear, which acts as the second input to the train, the sun gear being the first input. Two configurations considered for the DVT were the carrier-carrier and the carrier-ring. Each of these configurations was examined in detail before a particular configuration was selected.

Figure 4 is the schematic arrangement of the gears in the carrier-carrier configuration. In this type the carrier output of the first stage is connected with the carrier of the second stage. So, when the ring gear 1 is engaged, the carrier 1 carries a determined output, which is fed to the carrier of the second stage and this acts as the second input to the second stage. The same is true with the second and the third stages and hence a determined output is obtained from the carrier shaft of the last stage. The speed of the carrier for any stage can be calculated from the following relation.

$$\omega_C = \frac{\omega_S T_S + \omega_R T_R}{T_S + T_R}$$

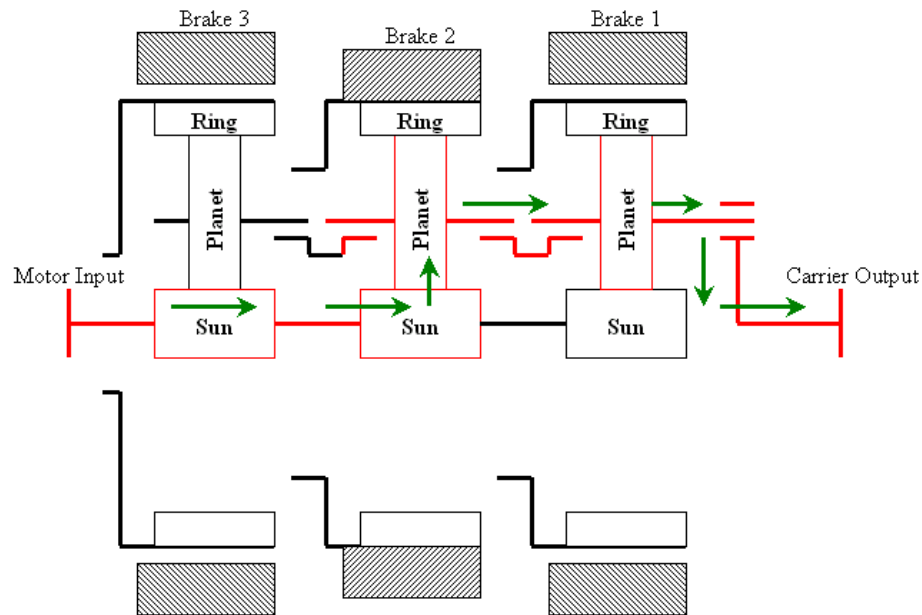


Figure 4 – Carrier-Carrier Configuration

N's represent the speed of the respective member and T's represent the number of teeth on each gear. Though this configuration was suitable for the system, the following were some of the complexities with this design.

- ✓ Interconnecting the carriers using suitable shaft couplings: With this approach the coupling between the carriers would be difficult to accomplish. Moreover it introduced complexities in the design of the carriers and housings.
- ✓ Supporting the carrier shafts in the housing with suitable bearings was another difficulty. This would make the assembly process very complex.
- ✓ With all the carriers connected, the support for the ring gear was to be made on the carrier shafts. This adds more loads on the carrier shafts and

again this increases the complexity of the assembly and the design of the housings.

- ✓ Two stages of the system would be “floating”. Hence compound reduction is not possible.

Considering all the above factors, the carrier-carrier configuration was not recommended for the prototype of DVT.

Figure 5 shows the schematic of the carrier-ring configuration. With this configuration the problems involved with the previous design are overcome to a great extent. The connection between the carrier and the ring is made with the help of involute splines. External splines on the carrier mesh with internal splines on the ring gear, thus functionally representing a single piece of shaft. Doing the carrier-ring assembly this way makes the assembly process simple.

Now, a bearing can be used to support the carrier shaft to the housing, which also acts as the support to the ring gears. Snap rings are used to restrain the components in the axial direction. An exploded view of the carrier-ring assembly can be found in the Figure 6. The splines used are to SAE standards. A detailed discussion on the design of the splines can be found in the later chapters. The carrier shaft is to be made hollow and also sufficiently large, for the sun gear to pass through. Because of the advantages of this design, a carrier-ring configuration was chosen for implementation in the DVT. The other issues like the design of the gears, carriers and splines is discussed in chapter 4.

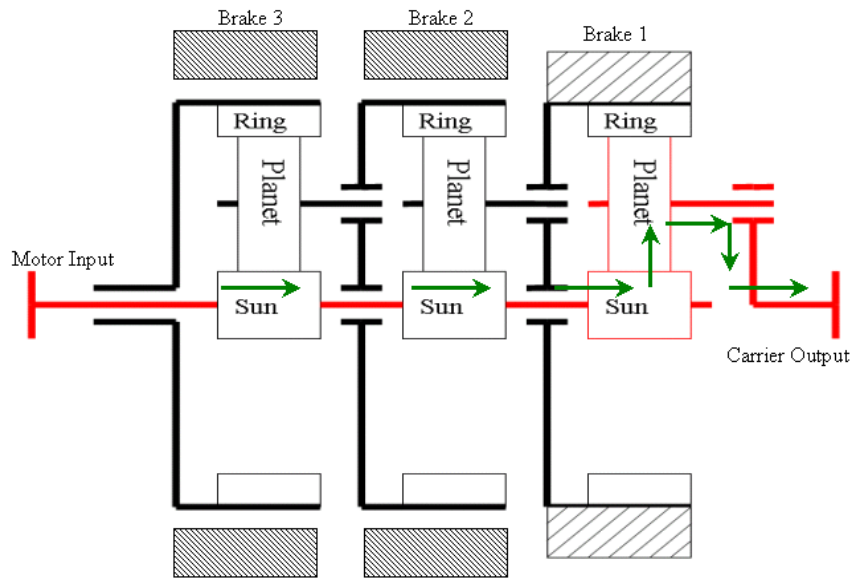


Figure 5 – Carrier-Ring Configuration

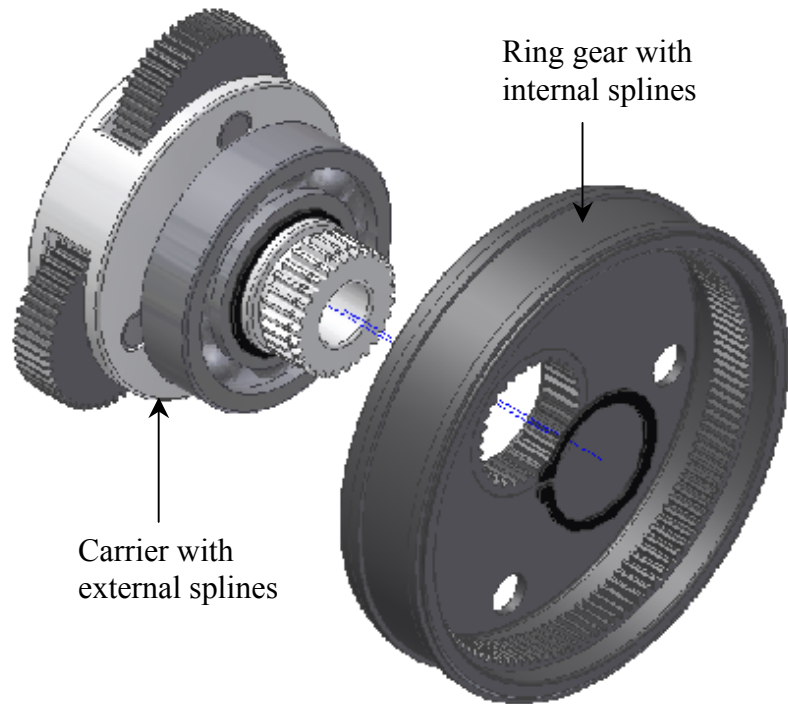


Figure 6 – Exploded View of a Carrier – Ring Configuration

2.4 Breaking Down the Design into Components

In any engineering design project, it is often necessary to break down the design task into sub tasks that can be easier to manage. In the development of the individual components, it is important to focus on the overall system performance and functionality. From the overall design specifications, the requirements of each single piece in the system are identified and all the components are designed based on those requirements. In this way the overall system requirements are satisfied and the system thus built can be guaranteed to be a well-engineered product. The following is the component-wise breakdown of the discrete variable transmission system. The list below does not include the issues related to the control of the DVT system and interfacing the system with the host computer, as the scope of this work is limited to the mechanical design part of the project.

- ✓ Individual gears viz., the sun, planet and the ring gears should be designed to meet the ratio as well as the load requirements. It is desirable to keep the overall size of each individual planetary gear train the same. This would help in the manufacturing of the carriers and also make the housing design simpler. Care should be taken to design gears that can be manufactured with standard tools, so that the cost of manufacturing is reduced.
- ✓ From the configuration of the DVT, the sun gear was one of the two inputs to all the three planetary gear train. Hence, a single piece shaft with

the sun gears cut them should be designed.

- ✓ Planet carriers should be designed based on the gear data. Carrier output shafts are splined as discussed in the DVT configuration and hence involute splines have to be designed based on the load information. Also the carrier shaft should provide enough room for the sun gears to pass through.
- ✓ Ring gears should be designed with shafts having internal splines, which can mate with their external counter parts on the carriers.
- ✓ The DVT housing, because of the nature of the design, is a split housing connected together with suitable bolts. Accommodations to be made for the brake mechanism interface with the DVT.
- ✓ Suitable bearings have to be selected for the shafts designed.
- ✓ A brake mechanism is used in DVT for the gear shifting. Hence detailed design of this brake mechanism has to be addressed. This includes the design of the band brakes, brake linkages, a slider-crank mechanism to actuate the braking mechanism, suitable support structure for accommodating the slider and the brake motor and support structure for the motor shaft. Refer [12] for a detailed discussion on gear shifting mechanisms.

For each of these components, a detailed manufacturing drawing has to be presented to the manufacturer. AutoDesk Inventor 6.0 was the modeling software used for this purpose. All parts to be manufactured can be modeled as a 3D part

in Inventor and a virtual assembly can be made which serves to verify the integrity of the parts. The drawing module in Inventor can be used to generate different drawing views. A detailed discussion of the CAD model representation of the DVT is made in chapter five.

2.5 Summary

This chapter presented a conceptual design for the Discrete Variable Transmission system. It addressed the baseline requirements derived from simulation results. The hardware for the DVT was discussed in detail. The concept of planetary gear trains and the working mechanism for such a gear train was presented. Several conditions of operation of these gear trains were discussed. Detailed discussion on the configuration for the DVT was made and a comparison of one design with the other was done. Design components were identified and laid out to aid in the detailed design process.

This chapter describes a detailed study of the discrete variable transmission with respect to the equations governing the motion of the system. Speed equations based on the kinematics and a torque analysis of the DVT system, using Newton's second law, is presented which describes the relation between the input, output and the brake torque. These final equations can be of interest to estimate the static and the dynamic brake torques that the braking mechanism has to generate in order to induce gear shifting. First a single stage planetary gear train is analyzed, which is then used for a three stage planetary gear set. In either case the friction between the gears is ignored and constant gear mesh conditions are assumed.

3.1 Speed Equations

Speed equations describe the kinematic relation between the different members of the system. Using this analysis, one can determine the speeds of every member of the gear train, given two inputs. It is worth noting that the sun, carrier and the ring gears rotate about the same axis and the planets rotate about their own axis, in addition to rotating about the axis of the sun gear.

From the configuration of the DVT system, recall that the sun gear is one

of the inputs to every planetary gear train (*a common sun shaft that is driven by the motor*). The other input is provided by the brake mechanism, which brings the angular velocity of a ring gear to zero. These two inputs determine the motion of all the members of the gear train. The carrier of each stage is connected with the ring of the next, making them rotate at the same speed and direction. The purpose of the following work is to derive a relation between the angular velocity of the input and the angular velocity of the output for each of the three gears. These equations are useful in sizing of the gears i.e., they are used to find the relative sizes of the gears. They are also of interest for the torque analysis in the next section to determine the torque relations.

The notations used in this study, 1,2 and 3 represent the planetary gear train of the respective stage. Equation 3.1 is the basic kinematic equation of a planetary gear train relating the carrier speed to the speeds of the sun and the ring gears. Given the speeds of the sun and the ring gears, one can determine the carrier speed. Refer to Figure 5 along with the discussion in this chapter.

$$\omega_C = \frac{\omega_S T_S + \omega_R T_R}{T_S + T_R} \quad (3.1)$$

First Gear: (Highest ratio 7:1)

When the system is in the first gear, i.e. when the brake B1 is engaged, ω_{R3} , the angular velocity of the third ring gear in the above equation is zero, and hence the output speed of the system is given by,

$$\omega_{C3} = \frac{\omega_{S3}T_{S3}}{T_{S3} + T_{R3}} \quad (3.2)$$

In this gear a maximum speed reduction of 7:1 and corresponding torque amplification is achieved.

Second Gear: (Ratio 4:1)

In the second gear, the brake B2 is engaged and hence ω_{R2} is zero. Hence the output of the second stage is given by,

$$\omega_{C2} = \frac{\omega_{S2}T_{S2}}{T_{S2} + T_{R2}} \quad (3.3)$$

Because of the carrier-ring configuration, the angular velocity of the third ring gear is also described by the above equation. Thus the final output from the system using (3.1) is given by,

$$\omega_{C3} = \frac{\omega_{S3}T_{S3} + \left(\frac{\omega_{S2}T_{S2}}{T_{S2} + T_{R2}} \right) T_{R3}}{T_{S3} + T_{R3}} \quad (3.4)$$

This is the final carrier speed for the second gear, with a total speed reduction of 4:1.

Third Gear: (Ratio 3:1)

In the third gear with the brake B3 engaged, ω_{R1} is brought down to zero resulting the first carrier output speed of,

$$\omega_{C1} = \frac{\omega_{S1}T_{S1}}{T_{S1} + T_{R1}} \quad (3.5)$$

$$\Rightarrow \omega_{C2} = \frac{\omega_{S2}T_{S2} + \left(\frac{\omega_{S1}T_{S1}}{T_{S1} + T_{R1}} \right) T_{R2}}{T_{S2} + T_{R2}} \quad (3.6)$$

The equation above gives the angular velocity of the second carrier. The final output speed of the DVT system for the 3:1 gear ratio is given by the following equation.

$$\Rightarrow \omega_{C3} = \frac{\omega_{S3}T_{S3} + \left(\frac{\omega_{S2}T_{S2} + \left(\frac{\omega_{S1}T_{S1}}{T_{S1} + T_{R1}} \right) T_{R2}}{T_{S2} + T_{R2}} \right) T_{R3}}{T_{S3} + T_{R3}} \quad (3.7)$$

It should be noted that all the sun gears are integral in a single shaft and hence, their angular velocities are always the same. ($\omega_{S1} = \omega_{S2} = \omega_{S3} = \omega_S$). The speed of the planet gears with respect to the axis of the sun at any time is given by [13],

$$\omega_P = \frac{\omega_S T_S - \omega_C (T_S + T_P)}{T_P} \quad (3.8)$$

In a particular stage, if the ring gear is engaged, the carrier speed of the previous stage is also zero and hence the total speed of the planet will be purely with respect to its own axis and is given by the equation (3.9) by putting ω_C in (3.8) as zero.

$$\omega_P = \frac{\omega_S T_S}{T_P} \quad (3.9)$$

A Pro-Mechanica working model of the three stages DVT was developed which served to verify these analytical speed equations and the torque equations

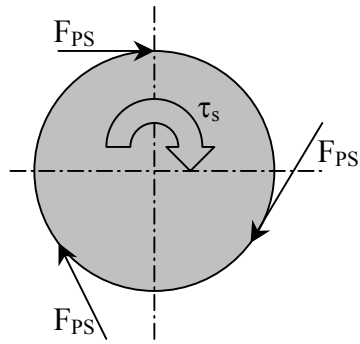
described in the next section. A detailed discussion of the dynamic model in Pro-Mechanica is presented in the chapter 5 of this thesis.

3.2 Torque Equations

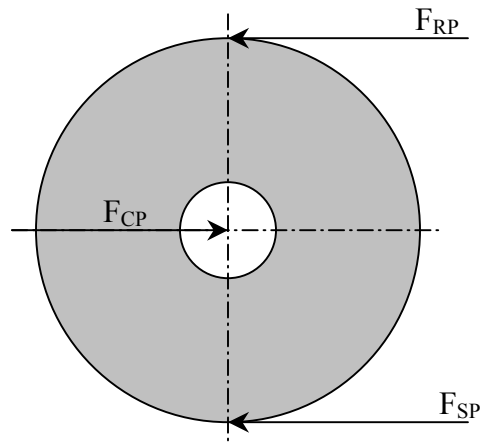
The purpose of this analysis is to describe in detail the dynamics of the DVT system. The equations that are described here are all steady state equations, i.e., they apply when the system is at a particular gear. As described earlier, these following equations can be used to determine the braking torque needed for the system. A free body diagram of each individual component is presented and a relation between the inputs and output are established. These equations play a major role in sizing the motor, sizing the transmission and determination of the required static and dynamic braking torques[‡].

A free body diagram representing the forces on the individual gears is shown in Figure 7. Three planets are used in the DVT system and hence the load is distributed evenly among them, provided the manufacturing errors are negligible. In addition to the forces and torques indicated on the figure, the sun, ring and the carrier have a reaction torque associated with them. Friction and viscous damping are some of the other components present that are beyond the scope of this analysis. Based on Figure 7, the following equations can be written for each member of a single planetary gear train using force and torque balance.

[‡] Acknowledgement to Kelley P. Brown, Dr. Sewoong Kim, Kalyana Ganti



(a) Sun Gear



(b) Planet Gear

Figure 7 – Free Body Diagram of a Single Planetary Gear Train

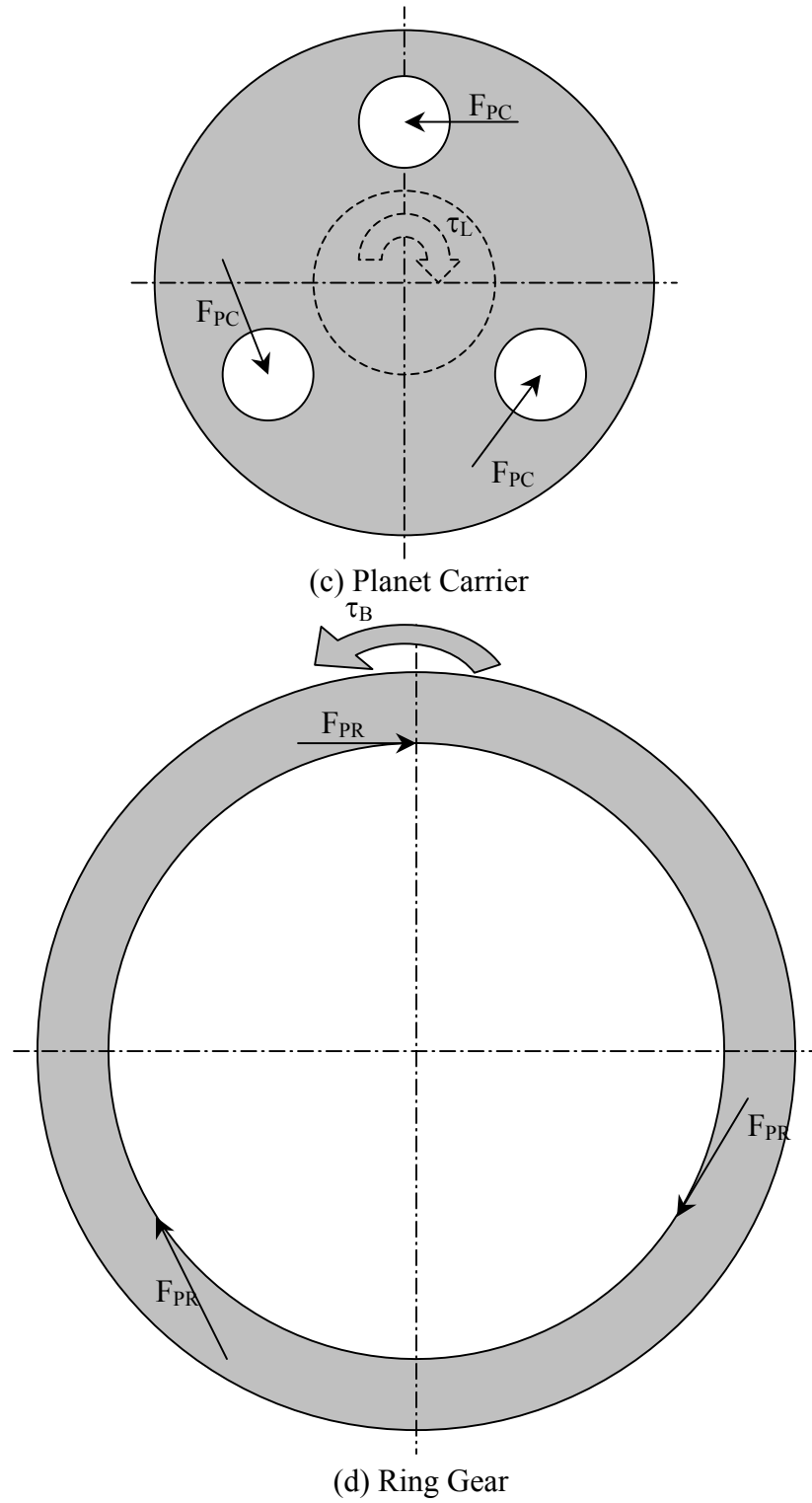


Figure 7 Continued

Sun Gear

$$\tau_S = J_S \frac{d\omega_S}{dt} + 3F_{PS} * r_S + \tau_{RS} \quad (3.10)$$

Planet Gear

$$r_P * (F_{SP} - F_{RP}) = J_P * \frac{d\omega_P}{dt} \quad (3.11)$$

$$F_{SP} + F_{RP} - F_{CP} = m_P * \frac{d\omega_C}{dt} * (r_S + r_P) \quad (3.12)$$

Ring Gear

$$3F_{PR} * (r_S + (2 * r_P)) = J_R * \frac{d\omega_R}{dt} + F_{BR} * (r_S + (2 * r_P) + r_{TH}) + \tau_{RR} \quad (3.13)$$

Planet Carrier

$$F_{PC} * (r_S + r_P) = J_C * \frac{d\omega_C}{dt} + \tau_{RC} + \tau_L \quad (3.14)$$

From the arrangement of the gears in a planetary gear train system we can deduce the following relations.

$$r_S + r_P = r_C \quad r_S + 2r_P = r_R \quad (3.15)$$

$$F_{BR} * (r_S + (2 * r_P) + r_{TH}) = \tau_B \quad (3.16)$$

Substituting (3.15) and (3.16) in the equations (3.10) through (3.14), we obtain the following equations, which govern the dynamics of a single planetary gear system.

$$\tau_S = J_S \frac{d\omega_S}{dt} + 3F_{PS} * r_S + \tau_{RS} \quad (3.17)$$

$$r_p * (F_{sp} - F_{rp}) = J_p * \frac{d\omega_p}{dt} \quad (3.18)$$

$$3F_{PR} * (r_R) = J_R * \frac{d\omega_R}{dt} + \tau_B + \tau_{RR} \quad (3.20)$$

$$F_{PC} * (r_C) = J_C * \frac{d\omega_C}{dt} + \tau_L + \tau_{RC} \quad (3.21)$$

The kinematic relations derived in the previous section are used in the above equations to solve for the torques in the system. The foregoing analysis is only for a single planetary gear system and suitable substitutions can be made to the final result to use it for a three stage planetary gear train. From (3.1),

$$\omega_C = \frac{\omega_S T_S + \omega_R T_R}{T_S + T_R} = a_1 \omega_S + a_2 \omega_R \quad (3.22)$$

where, $a_1 = \frac{T_S}{T_S + T_R}$ and $a_2 = \frac{T_R}{T_S + T_R}$. The planet speeds from (3.8) are

$$\omega_p = \frac{(\omega_S * T_S) - \omega_C (T_S + T_P)}{T_P}$$

Substituting for the carrier speed from (3.1) and simplifying,

$$\omega_p = \frac{(T_S - a_1 T_S - a_1 T_P) \omega_S + (-a_2 T_S - a_2 T_P) \omega_R}{T_P} = b_1 \omega_S + b_2 \omega_R \quad (3.23)$$

where, $b_1 = \frac{T_S - a_1 T_S - a_1 T_P}{T_P}$ and $b_2 = \frac{-a_2 T_S - a_2 T_P}{T_P}$

From (3.19),

$$F_{CP} = F_{SP} + F_{RP} - m_p * \frac{d\omega_C}{dt} * (r_S + r_P)$$

$$\Rightarrow F_{CP} = F_{SP} + F_{RP} - m_P * (a_1 \dot{\omega}_S + a_2 \dot{\omega}_R) * r_C \quad (3.24)$$

Substituting (3.24) in (3.21),

$$\begin{aligned} r_C [F_{SP} + F_{RP} - m_P * (a_1 \dot{\omega}_S + a_2 \dot{\omega}_R) * r_C] &= J_C * (a_1 \dot{\omega}_S + a_2 \dot{\omega}_R) + \tau_L + \tau_{RC} \\ \Rightarrow r_C (F_{SP} + F_{RP}) &= m_P * (a_1 \dot{\omega}_S + a_2 \dot{\omega}_R) * r_C^2 + \tau_L + J_C * (a_1 \dot{\omega}_S + a_2 \dot{\omega}_R) + \tau_{RC} \\ \Rightarrow (F_{SP} + F_{RP}) &= \frac{(m_P * r_C^2 * a_1 + J_C * a_1)}{r_C} \dot{\omega}_S + \frac{(m_P * r_C^2 * a_2 + J_C * a_2)}{r_C} \dot{\omega}_R + \frac{\tau_L}{r_C} + \frac{\tau_{RC}}{r_C} \end{aligned} \quad (3.25)$$

From (3.18),

$$\begin{aligned} r_P * (F_{SP} - F_{RP}) &= J_P * \dot{\omega}_P \\ \Rightarrow r_P * (F_{SP} - F_{RP}) &= J_P * (b_1 \dot{\omega}_S + b_2 \dot{\omega}_R) \\ \Rightarrow (F_{SP} - F_{RP}) &= \frac{(J_P * b_1)}{r_P} \dot{\omega}_S + \frac{(J_P * b_2)}{r_P} \dot{\omega}_R \end{aligned} \quad (3.26)$$

Solving equations (3.25) and (3.26) results in

$$F_{SP} = \left(\frac{(m_P * r_C^2 * a_1 + J_C * a_1)}{2 * r_C} + \frac{J_P * b_1}{2 * r_P} \right) \dot{\omega}_S + \left(\frac{(m_P * r_C^2 * a_2 + J_C * a_2)}{2 * r_C} + \frac{J_P * b_2}{2 * r_P} \right) \dot{\omega}_R + \left(\frac{\tau_L + \tau_{RC}}{2 * r_C} \right) \quad (3.27)$$

$$F_{RP} = \left(\frac{(m_P * r_C^2 * a_1 + J_C * a_1)}{2 * r_C} - \frac{J_P * b_1}{2 * r_P} \right) \dot{\omega}_S + \left(\frac{(m_P * r_C^2 * a_2 + J_C * a_2)}{2 * r_C} - \frac{J_P * b_2}{2 * r_P} \right) \dot{\omega}_R + \left(\frac{\tau_L + \tau_{RC}}{2 * r_C} \right) \quad (3.28)$$

Equations (3.28) and (3.29) represent the forces at the sun-planet mesh and the planet-ring mesh respectively in terms of the accelerations and the load torque. It can be seen from these equations that when the acceleration in the gear train is zero, the force values are purely a function of applied load, neglecting the effects of friction. Substituting these equations back in (3.17),

$$\tau_S = J_S \frac{d\omega_S}{dt} + 3 \left[c_1 \dot{\omega}_S + c_2 \dot{\omega}_R + c_3 \tau_L + c_4 \tau_{RC} \right] * r_S + \tau_{RS} \quad (3.29)$$

where,

$$c_1 = \left(\frac{m_P * r_C^2 * a_1 + J_C * a_1}{2 * r_C} + \frac{J_P * b_1}{2 * r_P} \right)$$

$$c_2 = \left(\frac{m_P * r_C^2 * a_2 + J_C * a_2}{2 * r_C} + \frac{J_P * b_2}{2 * r_P} \right)$$

$$c_3 = c_4 = \frac{1}{2 * r_C}$$

Substituting (3.28) into (3.20) yields,

$$\tau_B = 3(d_1 \dot{\omega}_S + d_2 \dot{\omega}_R + d_3 \tau_L + d_4 \tau_{EC}) r_R - (J_R * \dot{\omega}_R) - \tau_{RR} \quad (3.30)$$

where,

$$d_1 = \left(\frac{m_P * r_C^2 * a_1 + J_C * a_1}{2 * r_C} - \frac{J_P * b_1}{2 * r_P} \right)$$

$$d_2 = \left(\frac{m_P * r_C^2 * a_2 + J_C * a_2}{2 * r_C} - \frac{J_P * b_2}{2 * r_P} \right)$$

$$d_3 = d_4 = \frac{1}{2 * r_C}$$

Equations (3.29) and (3.30) represent the torques on the sun gear and the brake torque respectively. It should be noted that the brake torque that is represented by (3.30) is the holding torque that the brake system has to supply at any particular gear. The other kind of brake torque is the dynamic brake torque that is necessary to bring the ring gear to a zero angular velocity. Rearranging (3.29) and (3.30), the final dynamic equations for a single stage planetary gear train can be given as,

$$\tau_S = e_1 \dot{\omega}_S + e_2 \dot{\omega}_R + e_3 \tau_L + e_4 \tau_{RC} + \tau_{RC} \quad (3.31)$$

$$\tau_B = f_1 \dot{\omega}_S + f_2 \dot{\omega}_R + f_3 \tau_L + f_4 \tau_{RC} - \tau_{RR} \quad (3.32)$$

where,

$$e_1 = J_S + 3c_1 r_S$$

$$e_2 = 3c_2 r_S$$

$$e_3 = 3c_3 r_S$$

$$e_4 = 3c_4 r_S$$

$$f_1 = 3d_1 r_R$$

$$f_2 = 3d_2 r_R - J_R$$

$$f_3 = 3d_3 r_R$$

$$f_4 = 3d_4 r_R$$

These equations can be extended for a three stage planetary gear train with a carrier-ring configuration. For such a gear train, Figure 8 represents the internal

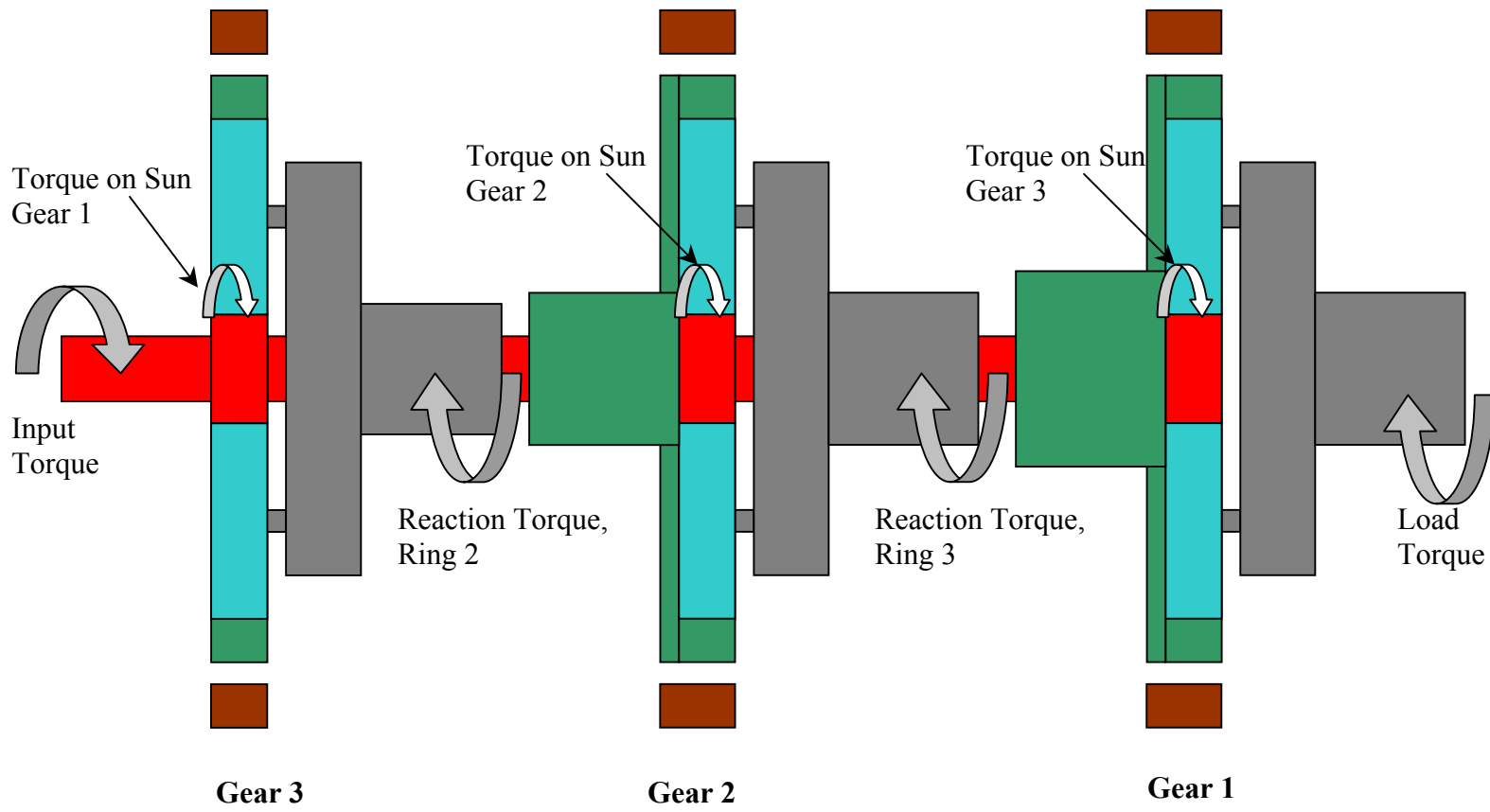


Figure 8 – Diagram of Internal Torques for a Three-Stage Planetary Gear Train

torques of the system. From Figure 8, the following relations can be established for each stage of the planetary gear train.

Stage 1

$$\tau_{RC1} = 0$$

$$\tau_{L1} = \tau_L$$

Stage 2

$$\tau_{RC3} = 0$$

$$\tau_{L2} = \tau_{RR1}$$

Stage 3

$$\tau_{RC1} = 0$$

$$\tau_{RR1} = 0$$

$$\tau_{L3} = \tau_{RR2}$$

From the kinematics of the system,

$$\omega_{C1} = \omega_{R2} \quad \omega_{C2} = \omega_{R3}$$

$$\omega_{S1} = \omega_{S2} = \omega_{S3} = \omega_S$$

These relations can be substituted back in (3.29) and (3.30) to obtain the following equations for the input and braking torques in each of the three gears of the DVT.

Gear 1

$$\tau_{S1} = e_{11} \dot{\omega}_{S1} + e_{12} \dot{\omega}_{R1} + e_{13} \tau_L + \tau_{S2} + \tau_{S3} \quad (3.33)$$

$$\tau_{B1} = f_{11} \dot{\omega}_{S1} + f_{12} \dot{\omega}_{R1} + f_{13} \tau_L - \tau_{RR3} \quad (3.34)$$

Gear 2

$$\tau_{S2} = e_{21} \dot{\omega}_{S2} + e_{22} \dot{\omega}_{R2} + e_{23} \tau_{RR3} + \tau_{S1} + \tau_{S3} \quad (3.35)$$

$$\tau_{B2} = f_{21} \dot{\omega}_{S2} + f_{22} \dot{\omega}_{R2} + f_{23} \tau_{RR3} - \tau_{RR2} \quad (3.36)$$

Gear 3

$$\tau_{S3} = e_{31} \dot{\omega}_{S3} + e_{32} \dot{\omega}_{R3} + e_{33} \tau_{RR2} + \tau_{S1} + \tau_{S2} \quad (3.37)$$

$$\tau_{B3} = f_{31} \dot{\omega}_{S3} + f_{32} \dot{\omega}_{R3} + f_{33} \tau_{RR2} \quad (3.38)$$

With the help of the above equations, at any particular gear, the required amount of braking torque can be calculated. With one of the gears locked, the motion of every other member of the gear train is deterministic and one can determine the amount of dynamic braking torque that is needed to switch between the gears. The validity of these equations is verified using a Pro-Mechanica dynamic simulation model for a single and three stage planetary gear systems. These equations are also very helpful in sizing the motor and the gear train components, which will be discussed in detail in the following chapters.

3.3 Summary

This chapter examined the speed and torque equations governing the kinematics and dynamics of the DVT system, which will be useful for sizing the components of the system. The losses in the system viz., the friction, viscous damping etc., were not considered. All the equations presented here are for the steady state condition.

This chapter discusses the detailed design of the DVT system. Specific components that will be discussed here are the gears, carriers and splines, housing and the brake mechanism. The tolerances and fits corresponding to the components designed will be presented. Finite element analyses of the gears that are designed are discussed in the later chapters.

4.1 Sizing of the Gears

Having established the ratio requirements and the configuration for the DVT, the initial sizing of the gears is centered on meeting the speed ratios. An attempt was made to use commercially available planetary gear trains coupled to each other. Almost every planetary gear train that is available is a single stage reduction in which the ring gear is grounded to the housing. Moreover, for a commercially available gear train the housings and supports would have to be custom made. Because three individual commercially available planetary gear trains could not meet the overall ratio requirements of the DVT system and also because of the use of a brake band to stop the ring gear for the gearshift, a custom design was proposed. The kinematics that governs the system is used to determine the relative sizes of each gear for the three stages. This provides us

with enough information to choose a gear (in the case of standard gears) based on the torque and the power that the gear is required to handle. In case of a non-standard gear, the tooth profile of the gear has to be modified to fit a non-standard center distance and to avoid interference problems. These issues will be discussed in detail in the later sections. The focus of this section is on determining the relative gear sizes for the required speed ratios.

As discussed in chapter 3, the kinematic equation that relates the speeds of the planetary gear train members is

$$\omega_C = \frac{\omega_S T_S + \omega_R T_R}{T_S + T_R} \quad (4.1)$$

Where,

T 's represent the number of teeth on the sun and ring gears

ω 's represent the angular velocities of the planet carrier, sun and the ring

Recall that the DVT system will have the motor input to the sun gear and the brake mechanism input to the ring gear as the two inputs to the planetary gear train and the final carrier shaft as the output of the system (*Refer to figure 5*).

Equation 4.1 is used to for the sizing of the gears. The following is the procedure that describes an example calculation that was made.

Consider that the system is in the first gear i.e. 7:1 reduction. The speed of the ring gear of that stage is zero. Using equation 4.1, in this case, the ratio of the final carrier and sun speed is given by,

$$\frac{\omega_{C3}}{\omega_S} = \frac{T_S}{T_S + T_R} = \frac{1}{7} \quad (4.2)$$

Rearranging the equation, it can be seen that $T_R = 6T_S$. Hence, for a speed reduction of 7:1, the number of teeth on the ring gear has to be six times the number of teeth on the sun. Once the size of the sun and the ring gears are established, the number of teeth on the planet is determined from,

$$T_P = \frac{T_R - T_S}{2} \quad (4.3)$$

The number of teeth on one of the gears is set arbitrarily and the sizes of the other gears are determined from the above relations. The similar method is used to size the gears of the first and the second stages. In that case, the carrier speed of the one stage should be substituted for the ring gear speed of the next stage in equation 4.1. Using this procedure, the following were the approximate relative gear sizes.

$$\text{First stage: } T_R = 8T_S$$

$$\text{Second stage: } T_R = 7T_S$$

$$\text{Third stage: } T_R = 6T_S$$

Once the module (*which is the ratio of the pitch diameter and the number of teeth*) for the gears is selected, one can determine the pitch diameters of the gears, the addendum, dedendum, base diameter and other gear dimensions using standard relations available in gear handbooks [14]. If standard gears were to be employed for the design, the relative sizes of the gears and the carriers would be

different from each other, which would increase the manufacturing cost of the system. With this in mind, the center distance on all the carriers was made the same (1.375 inches). Hence the gear design was dependent on this value apart from meeting the ratio requirements. As a part of the specification of the design requirement, the overall size of the DVT system should be compatible with the volumetric space of the TITAN 3 manipulator. This imposed a size constraint on the pitch diameter of the ring gear to be 5". Considering all the above factors, the gears were designed to the numbers specified in the appendix. Due acknowledgement is given to Mr. George Bowers whose expertise in gear and transmission system design played a vital role in sizing of the gears and detailing the system. Figure 9 shows a snap shot of the sun gear.

It can be seen from the specifications of the gears that the gears are non-standard. In the case of non-standard gears, the center distance between the two gears is not just the average of the pitch diameters. Non-standard gears are adopted in situations where the two gears are required to fit a predetermined center distance or in cases where there are problems of interference between the pinion and the gear tooth. Although the interference problems could be resolved by undercutting, which is removal of the interfering metal by the cutter when the teeth are generated, it leads to the weakening of the pinion tooth[15]. To avoid these problems, non-standard gears were introduced. (*Refer appendix for more on non-standard gears.*) The two common non-standard gear systems are the extended center distance system and the long and short addendum. There are



Figure 9 – The Finished Input Shaft

several systems of non-standard gearing and some of them require a special cutting tool, which often results in an increase in the manufacturing cost. The gears used in this system, even though non-standard, were within the capability of being manufactured by Ann Arbor Gear Technologies, the company to which the manufacturing was contracted. All the sun gear was made integral with the input shaft, which avoids the need for any shaft couplings. Because of this reason, the diameter of the input shaft was limited by the root diameter of the sun gears. Ring gears were designed with shafts having internal splines that could mate with their external counter parts on the carrier of the previous stage. An exception to this is the first ring gear, which has a smooth bore shaft.

The material for the gears is SAE 4340 steel, which has a carbon content of approximately 0.4%. Given that the hardness of the gears depends more on the heat treatment than the composition, the gears blanks were heat treated (*quenched and tempered*) so that a hardness of 32-36 RC is obtained. Figure 10[14] (pg 10-3) shows relative hardness levels for steel and iron gears. This was subsequently followed by the machining of the gears and cutting the gear teeth to the final dimensions. Finally the gears were nitrided, which is the process of case

Table 10-2. Relative-hardness Levels for Steel or Iron Gears

Hardness		Machinability	Comments
Brinell	Rockwell C		
150-200	...	Very easy	Very low hardness. Minimum load-carrying capacity
200 250	... 24	Easy	Low hardness, moderate load capacity. Widely used in industrial gear work
250 300	24 32	Moderately hard to cut	Medium hardness. Good load capacity. Widely used in industrial work
300 350	32 38	Hard to cut, often considered limit of machinability	High hardness. Excellent load capacity. Used in lightweight, high-performance jobs
350 400	38 43	Very hard to cut. Many shops cannot handle	High hardness. Load capacity excellent provided heat-treatment develops proper structure
500 550	51 55	Requires grinding to finish	Very high hardness. Wear capacity good. May lack beam strength
587	58 63	Requires grinding	Full hardness. Usually obtained as a surface hardness by case carburizing. Very high load capacity for aircraft gears, automobile gears, trucks, tanks, etc.
	65 70	May be surface-hardened after final machining	Superhardness. Generally obtained by nitriding. Very high load capacity

Figure 10 – Relative Hardness Levels for Steel and Iron Gears

hardening alloy steel that depends on absorption of nitrogen into the steel. For nitriding the gears, the parts are heated in special containers (temperature of 1050°F in this case) through which ammonia gas is passed. The nitrogen that splits from ammonia reacts with the steel and penetrates the surface of the gear forming nitrides. The advantages offered by the nitriding process are very high surface hardness, high fatigue strength and high resistance to abrasion. The regions of the gears that are not to be nitrided (e.g. the region on input shaft where the bearing interfaces) are masked with a copper plate or other suitable medium. A finite element model for the gear teeth was performed to ensure the strength of the gears designed.

4.2 Design of Planet Carriers

Planet carriers, in the present configuration, serve the purpose of transmitting the output torque of one stage to the ring gear of the next stage. They also accommodate the planet gears, which are in mesh with both the ring and the sun gears. Care must be taken to design the carrier shaft for the conditions of torque and the bending loads (*due to any shaft misalignments*). The design configuration calls for the hollow carrier shaft for the first and second stages, which allows the sun gear shaft to pass through. Another important design consideration was achieving the carrier-ring configuration. Although there were many possible ways in which the carrier could be coupled with the ring gear, involute splines were found suitable for the design. Involute splines are

stronger than straight-sided splines and are easier to cut and fit. They are available in standard pressure angles of 30° and 45° . Involute splines have certain advantages, which make them increasingly popular in transmission system applications. They are [16],

- ✓ Maximum strength at the base of the tooth.
- ✓ Accuracy of spacing and the equalizing of bearing stresses among the teeth.
- ✓ Elimination of the need for grinding due to the smooth cutting action of the gear hob.

According to the SAE handbook, for carrying of any load or to obtain stability, there is seldom need to have a spline longer than its pitch diameter. A fillet root side fit was used for this design. The following sections discuss the detailed design procedure for one of the carriers.

4.2.1 The Final Carrier

As an example of the design procedure used for the carriers, the final carrier (*the one used for the third set planetary gear train*) is considered here. Figure 11 shows the 3D model of the final carrier of the DVT system. As mentioned earlier, involute splines are used for coupling the carrier with another transmission element, which in this case is the final reduction input shaft. Before a standard spline could be chosen from the catalog, one should have an estimate of the diameter of the shaft. To do this one has to examine the loading conditions

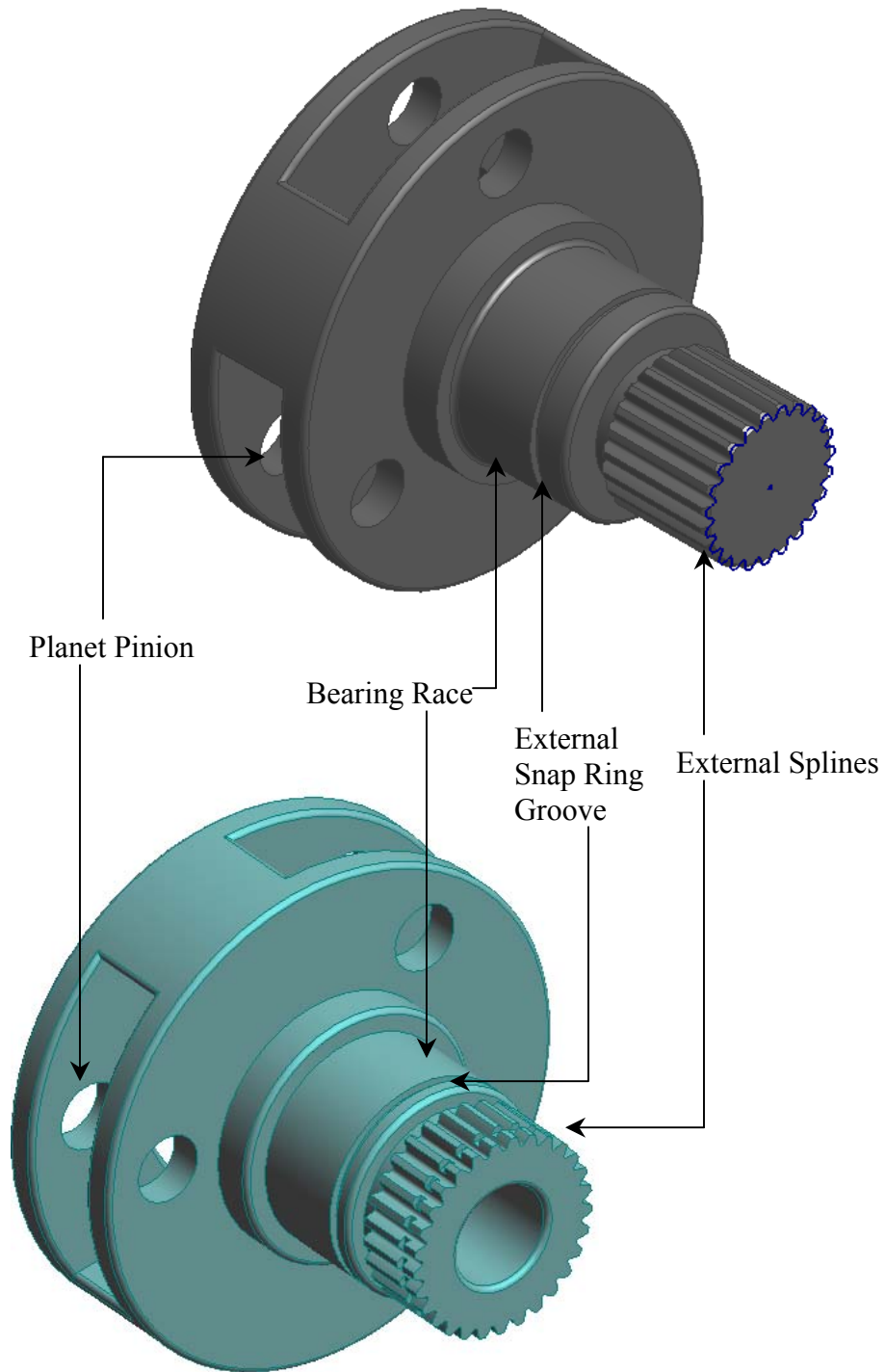


Figure 11 – DVT Carriers

to which the shaft is subjected. Since the carrier shaft is predominantly subjected to torsion, the following formulas were used to determine the diameter of the solid carrier shaft. Maximum *shear stress theory* and *von mises theory* were used to estimate the shaft. The shaft diameter according to these theories is given by,

Maximum Shear Stress Theory

$$D = \left(\frac{32.T.N_{FS}}{\pi.S_{YP}} \right)^{1/3} \quad (4.4)$$

Von Mises Theory

$$D = \left(\frac{27.71.T.N_{FS}}{\pi.S_{YP}} \right)^{1/3} \quad (4.5)$$

where,

T is the torque carried by the shaft

N_{FS} is the factor of safety

S_{YP} is the yield point stress of the material.

The input to the DVT viz., the sun gear is coupled with the motor that has a peak torque rating of 12N-m. With a 7:1 speed reduction, the carrier output shaft experiences a torque of 84N-m. The material of the carrier is 7075 Aluminum alloy with a yield stress of 542 Mpa (78.6 psi). A factor of safety value of 4 is used in the design calculations. Hence, using the maximum shear stress theory (*equation 4.4*), the diameter of the carrier shaft was estimated to be 0.7488 inches. A conservative estimate of 1 inch was used, which also is a standard shaft diameter. This diameter forms the basis for the spline selection. Figure 12 shows

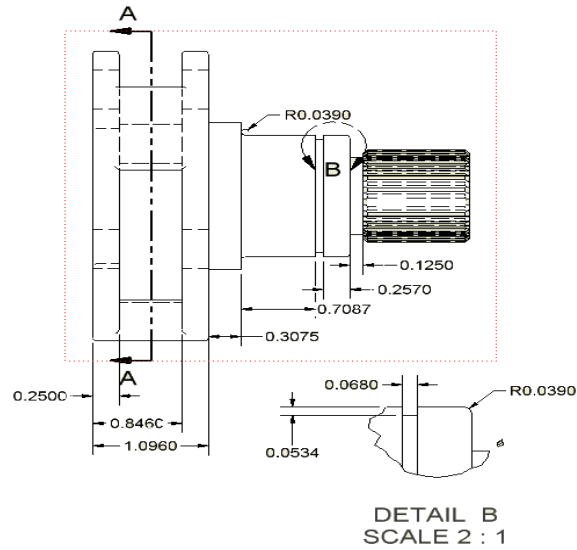


Figure 12 – Final Carrier Dimensions

the dimensions for the final carrier. In the case of first and second stage carriers, the carrier shaft is hollow, to allow for the sun gear shaft to pass through. The inner diameter of the hollow shaft was chosen to be 0.75 inches, which is greater than the major diameter of the final sun gear. The external diameter of the carrier shaft is determined using [18],

$$D = \left(\frac{32.T.N_{FS}}{\pi.(1 - R_D^4).S_{YP}} \right)^{1/3} \quad (4.6)$$

R_D represents the ratio of the hollow shaft (ratio of the inner diameter to the outer diameter). All the other terms are same as that for the solid shaft discussed before. With the diameter of the output shaft determined, an external spline that has a minor diameter of approximately 1 inch was chosen from the SAE spline catalog[17]. The spline used in this design has a 30° pressure angle and a 20/40

spline pitch with a major diameter of 1.2 inches. Figure 13 shows a section from the catalog, indicating the spline selection. The length of the spline according to the SAE standards is calculated using[16],

$$L = \frac{D_{re}^3}{D_p^2} \quad (4.7)$$

D_{re} refers to the minor diameter of the external spline and D_p refers to the pitch diameter of the spline. The length of the spline was computed as 0.8325 inches, which was rounded to 1 inch. By choosing this spline length, the strength of the spline teeth in shear is the same as the shaft strength in shear. Because of the use of splines on the carrier shaft, the output shaft of the DVT is to be stepped up to be more than the major diameter of the external spline so as to support it by a bearing. Hence a diameter of 1.5 inches was used. A bearing selection was made based on this shaft diameter value. The bearing chosen was the 208K radial ball

30 DEG PRESSURE ANGLE

TABLE 34-30 DEG PRESSURE ANGLE, FILLET ROOT SIDE FIT, 20/40 SPLINE PITCH

Internal and External	Internal (see Drawing Date)						External (see Drawing Date)										
	D Pitch Dia.	D _b Base Dia.	D _{Fi} Major Dia. Max.	D _{Fi} Form Dia.	D _i Minor Dia.	s_v Min. Eff. Circ. Space Width 0.0785 Notes c & d	t_v Max. Eff. Circ. Tooth Thickness 0.0785 Notes e & f			D _o Major Dia.	D _{Fe} Form Dia.	D _{re} Minor Dia. Min.					
Tolerance in Ten Thousandths	2	3.1	4.2	5.1	6.1	Max. Actual Circ. Space Width For Tolerance Class			Min. Actual Circ. Tooth Thickness for Tolerance Class			14.1	17.1	18.2			
						7	6	5	4	4	5				6	7	
						s ₂	s ₆	s ₅	s ₄	t ₄	t ₅	t ₆	t ₇				
			Note f		Note e	Notes a & b						Note g	Note e	Note f			
					+ .50 - .50									+ .50 - .50			
21	1.050000	0.9093267	1.155	1.104	1.000	0.0841	0.0824	0.0813	0.0805	0.0765	0.0757	0.0746	0.0729	1.100	0.996	0.935	
22	1.100000	0.9526279	1.205	1.154	1.050	0.0841	0.0824	0.0813	0.0805	0.0765	0.0757	0.0746	0.0729	1.150	1.046	0.985	
23	1.150000	0.9959292	1.255	1.204	1.100	0.0842	0.0825	0.0814	0.0805	0.0765	0.0757	0.0745	0.0728	1.200	1.096	1.035	
24	1.200000	1.039230	1.305	1.254	1.150	0.0842	0.0825	0.0814	0.0805	0.0765	0.0756	0.0745	0.0728	1.250	1.146	1.085	
25	1.250000	1.082532	1.355	1.304	1.200	0.0842	0.0825	0.0814	0.0805	0.0765	0.0756	0.0745	0.0728	1.300	1.196	1.135	

Figure 13 – Spline Selection

bearing having a bore diameter of 1.5748 inches.

The other issue to be considered here is to restrain the carrier shaft to the bearing, which is restrained in the DVT housing. Retaining rings (*snap rings*) and shaft shoulders are used for this purpose. Retaining rings can be thought of as a spiral spring in tension that fits into a groove on the shaft. They can withstand very high axial loads. They have ears, which can be expanded or contracted during the assembly. They require special tools (*pliers*) for this operation. Generally they are made of hardened steel and can be purchased as a standard item from the manufacturer's catalog. Figure 14 shows the two commonly used snap rings. The external snap rings are used on the shafts and the internal snap rings are used in the housings. The snap ring required is selected based on the shaft diameter and the bearings selected. Shaft shoulders on the other hand are built integral with the shaft. It is just a step-up in the diameter of the shaft. Care must be taken in designing the snap ring grooves on the shaft and the shaft shoulders, as these are potential regions of stress concentration on the shaft. This was taken into account during the design process and fillets were used

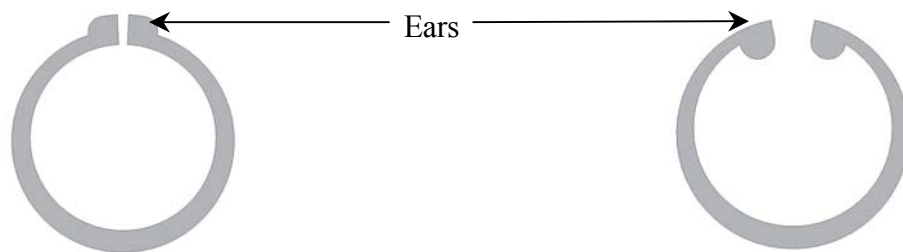


Figure 14 – Snap Rings

in the shaft where there was a change in the shaft cross section. The tolerance values on the shaft are determined based on the bearing selected and the snapping that is used. This is discussed in the next section.

4.2.2 Tolerances and Fits

A tolerance is the total permissible variation in the size of a part. *Unilateral* and *Bilateral tolerancing* and *Limit dimensioning* are the commonly used tolerancing methods. Tolerances and fits play a vital role in the assembly of different components. It is not a random process and requires consideration on the design, production cost, and machines to be used. It is preferable to keep the tolerance numbers larger wherever possible, (without compromising performance) as tighter tolerance increases manufacturing costs. So care must be taken to account for these factors.

Figure 15 shows a section of the catalog corresponding to the bearing

Light • 200, 5200, 7200WN Series								
Basic Bearing Number	Shoulder Diameters							
	shaft, S		housing, H					
	max.	min.	max.	min.	max.	min.	max.	min.
	in.	mm.	in.	mm.	in.	mm.	in.	mm.
205	1.22	31.0	1.14	29.0	1.81	46.0	1.78	45.2
206	1.47	37.3	1.34	34.0	2.21	56.1	2.16	54.9
207	1.72	43.7	1.53	38.9	2.56	65.0	2.47	62.7
208	1.94	49.3	1.73	43.9	2.87	72.9	2.78	70.6
209	2.13	54.1	1.94	49.3	3.07	78.0	2.97	75.4

Figure 15 – Shaft and Housing Shoulder Tolerances

that is chosen. Tolerance values for the carrier were determined from the Torrington Bearing Catalog[19]. The table represented in Figure 15 gives the radial tolerances of the shoulder diameter on the shaft and the housing. The same procedure is followed in determining the tolerance values for the width and depth of the snap ring grooves on the shafts. A section from the snap ring manufacturers catalog[20] is shown in Figure 16. As for the other tolerance values, e.g. the tolerance values of the shaft diameter and width where the bearing interfaces, the type of fit required is first obtained from the Torrington catalog. The application for which the bearing is used determines the type of fit. After the type of fit is obtained, the tolerance value corresponding to that fit is obtained. Refer to Figure 17. Using this chart, a bearing-shaft fit of k5 and a bearing-housing fit of H6 was chosen for the design. This results in an interference fit between the shaft and the bearing bore and a mean-loose fit between the bearing and housing.

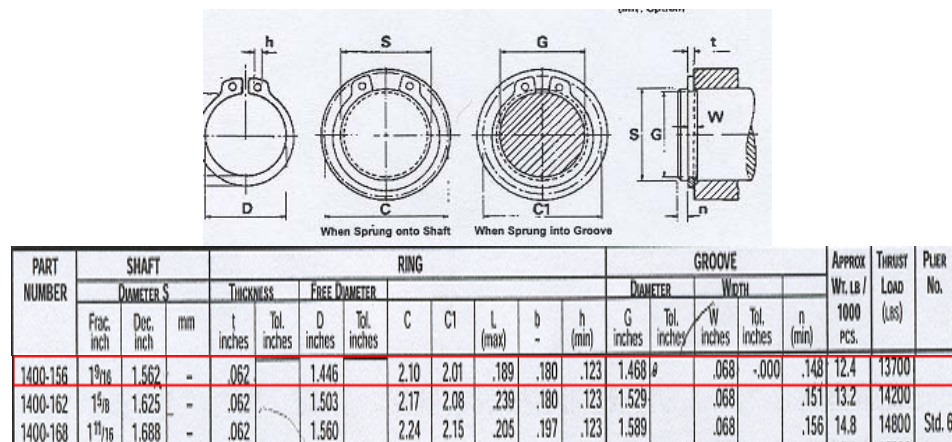


Figure 16 – Snap Ring Tolerance Values

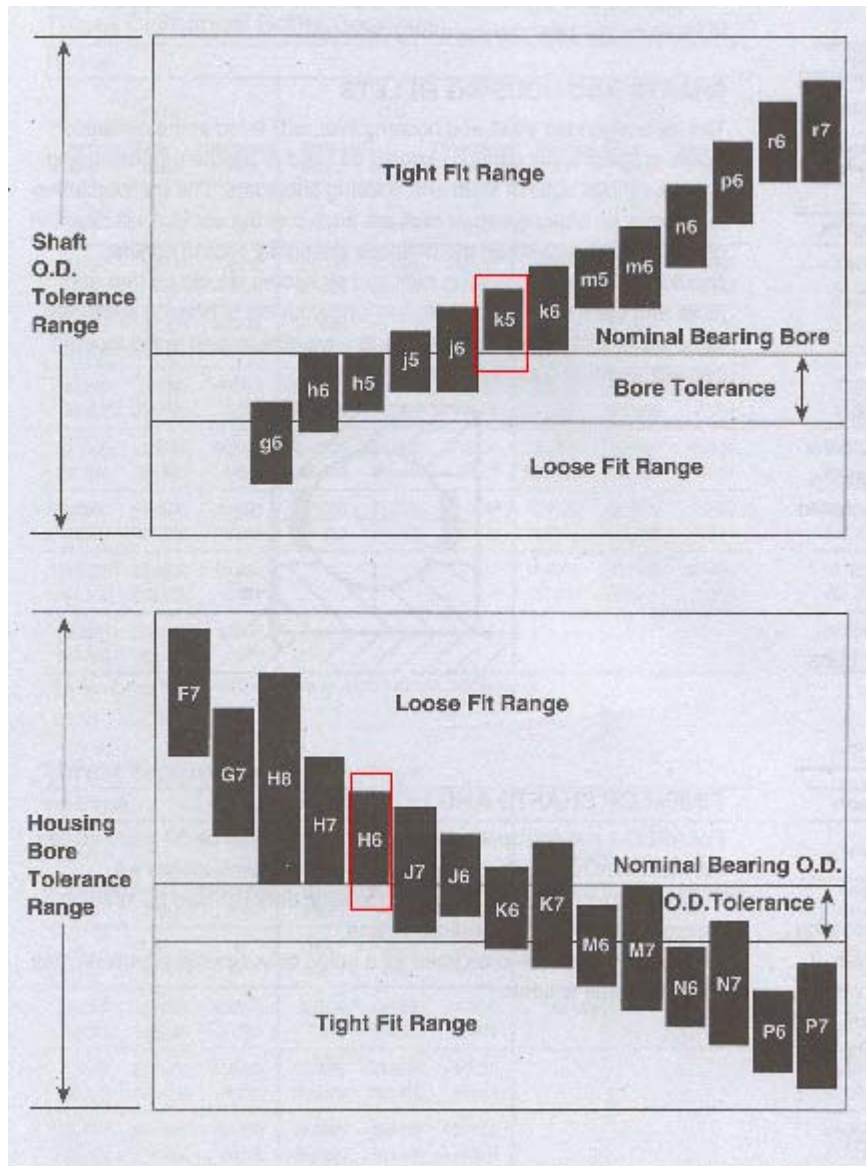


Figure 17 – Ranges of Shaft and Housing Fits

Ball Bearings (For all nominal diameters)			Operating Conditions	Examples
Loads		Shaft Tolerance Symbol		
Lower Load Limit	Upper Load Limit			
INNER RING ROTATING				
0	$C_e^{(7)}$	g6	Inner ring to be easily displaced on shaft	Wheels Non-rotating shafts
0	C_e	h6	Inner ring does not need to be easily displaced	Tension pulleys
INNER RING STATIONARY				
0	$0.07C_e$	j6⁽²⁾	Light loads	Electrical apparatus Machine tools Pumps Ventilators Industrial trucks
$0.07C_e$	$0.15C_e$	k5	Normal loads	Electrical motors Turbines Pumps Combustion engines Gear transmissions etc.

Operating Conditions		Examples	Housing Tolerance Symbol ⁽¹⁾	Outer Ring Displaceable Axially
OUTER RING STATIONARY				
Shock loads, temporary complete unloading		Heavy rail vehicles	J6	Yes, normally
All loads	One-piece housing	General applications Heavy rail vehicles	H6	Easily
	Radially split housing	Transmission drives	H7	Easily
Heat supplied through shaft		Drier cylinders	G7	Easily

Figure 17 Continued

It should be noted that all the tolerance values comply with the ABEC (*American Bearing Engineers committee*) 1 standard. Other ABEC standards are 3, 5, 7 and 9 and as the standard number increases, the tolerance values become tighter. The tolerance numbers corresponding to the k5 and H6 fits is obtained from the Figure 18. Another design element as a part of the carrier design is the sizing of the pins on which the planets ride. Needle bearings are used to support the planet pinions on the carrier. Use of two carrier cheeks to support the pins gives a better support as opposed to the cantilevered pin. The material between the two carrier cheeks was made so that enough clearance is available for the planet gears.

4.3 Bearing Selection

Bearings of one type or the other are used to provide support to the rotating member of the machinery. All bearings are manufactured to standard

SHAFT		cylindrical roller bearings, see pages E29, E30 and E31.																								
Bearing Bore	Nominal (max.) Over	Tol. +0 To	g6			h6			h5			j5			j6			k5			k6			m5		
			Shaft Dia.	Fit		Shaft Dia.	Fit		Shaft Dia.	Fit		Shaft Dia.	Fit		Shaft Dia.	Fit		Shaft Dia.	Fit		Shaft Dia.	Fit		Shaft Dia.	Fit	
mm	mm	mm	in.	in.	in.	in.	in.	in.	in.	in.	in.	in.	in.	in.	in.	in.	in.	in.	in.	in.	in.	in.	in.	in.	in.	in.
18	30	-4	-3	-8	8L 1T	0	-5	5L 4T				+2	-2	2L 6T	+4	-2	2L 8T	+4	+1	8T				+7	+3	3T 11T
		-10	-7	-20	20L 3T	0	-13	13L 10T				+5	-4	4L 15T	+9	-4	4L 19T	+11	+2	21T				+17	+8	8T 27T
30	50	-4.5	-4	-10	10L 0.5T 25L 3T	0	-6	6L 4.5T 16L 12T				+2	-2	2L 6.5T 5L 18T	+4	-2	2L 8.5T 5L 23T	+5	+1	11T 9.5T 2T 25T	+7	+1	11T 11.5T 2T 30T	+8	+4	4T 12.5T 8T 32T
50	80	-6	-4	-11	11L 2T 29L 5T	0	-7	7L 6T 19L 15T				+2	-3	3L 8T 7L 21T	+5	-3	3L 11T 7L 27T	+6	+1	11T 12T 2T 30T	+8	+1	11T 14T 2T 36T	+9	+4	4T 15T 11T 37T
80	120	-8	-5	-13	13L 3T 34L 8T	0	-9	9L 8T 22L 20T				+2	-4	4L 10T 9L 26T	+5	-4	4L 13T 9L 33T	+7	+1	11T 15T 3T 38T	+10	+1	11T 18T 3T 45T	+11	+5	5T 19T 13T 48T

Figure 18 – Shaft Tolerance Values Based on the Grade of Fit

sizes and must be fitted into the assembly just as the manufacturer supplies them. For the current design the required bearings were purchased from the Torrington Company and their bearing catalog[19] served as the guide for the selection of the right bearing. Bearings can be classified into many different types viz., ball bearings, roller bearings, taper roller bearings etc., depending upon the application and the loading conditions to which it is subjected.

Single row deep groove ball bearing (*Conrad type*) is the most widely used bearing of the rolling types of bearing. Figure 19 shows a cross section of this type of bearing. The balls in this bearing roll in the grooves in both the inner and outer races. It is because of these grooves that this bearing is capable of holding axial as well as radial loads. It can support axial loads in either direction. Since the DVT is subjected to radial loads predominantly and very little thrust loads, this bearing is found suitable. These bearings can be a non-filling slot type (*identified by suffix K in the catalog*) or filling-slot type (*identified by suffix W*). The former has an uninterrupted raceway shoulders and hence capable of supporting radial, thrust or the combined loads whereas the later is limited in its

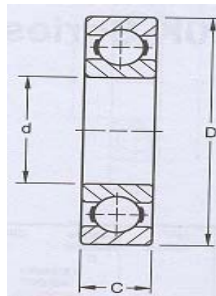


Figure 19 – Single Row Deep Groove Ball Bearing

thrust load capacity. Both these bearings are capable of being mounted with or without the use of locknuts. Two bearings at the either ends of the DVT, one supporting the final carrier and the other supporting the first ring gear, are required to be sealed, which prevents foreign matter to enter the bearing area and also the lubricant from leaking out of the system. It should be noted that the intermediate bearings are well packaged within the system and so the lubrication of the bearings is provided by the oil circulating inside the housing, which is not the case with the bearing supporting the first ring gear. Therefore sealed bearings were preferred which have the lubricant packed within them.

The shaft diameters on the stepped carrier shaft was set to be 1.5 inches as discussed in the carrier design and a radial ball bearing was selected based on this number. The bearings used in this design are the light series 208K for all the carrier shafts and 209K for the first ring gear. The input shaft is supported using a single bearing on the inside of the first ring gear, which acts as the housing for this bearing. Recall that the diameter of the input shaft is 1/2inch and hence an extra small series of bearings, SK5, was selected as the support for the input shaft. For the bearings selected, a simple life calculation was performed according to the guidelines specified in the Torrington catalog. A sample of such a calculation for the 208K bearing is shown below. The basic equation for life of a ball bearing in hours is given by,

$$L_{10} = \frac{16667}{N} \left[\frac{C_E}{P} \right]^3 \text{ Hours} \quad (4.8)$$

C_E and P refers to the extended dynamic load rating of the ball bearing and the equivalent radial load on the bearing respectively. N refers to the operating speed in r.p.m. With a factor of safety of 1.2, the value of P is approximated to be 720lbs. Considering the worst case operating conditions, an N value of 1600 is chosen. Using these numbers and the above formula, the approximate bearing life is 16000 hours.

As for the tolerances, the tolerance grades established by the American Bearing Engineers Committee (ABEC) was used to determine the various values. The most commonly used standard is the ABEC 1 and this is used for the current design. Other grades available are 3,5,7 and 9. As the grade increases the tolerance value becomes smaller. The higher grades are normally used for super precision applications such as aircraft control, high precision instruments and machine tools. The shaft tolerance and housing tolerance determined based on these standards are described in the respective sections.

4.4 DVT Housing

The function of the housing assembly is to form a strong base for the bearings, which support the shafts and gears and to provide an environment where a lubricant can be used to lubricate and cool the various transmission components. The housing is also used to mount and support various other components such as accessories and parts common to the gearing. In most of the transmission systems, the lubricant is contained entirely within the housing.

Having selected the bearings and the configuration of the system, the next task ahead is to design the support structure. The design must be sufficiently rigid so that any external loads do not affect the operating position of the gears[21].

Housings can be either one piece or split housing. One-piece housings are always stronger and more rigid than split housings. However, in the case of the DVT, as is the case with any complex machinery, one-piece housing was impossible due to the assembly requirements. Hence it was decided to make the DVT housing unit as an axially split housing fastened together with steel bolts (1/4-20's), eight at each interface. An effort was made to design the housings as small as possible. As a result, the input shaft was supported with a bearing that is supported inside the shaft of the first ring gear. This eliminated the need to have a separate housing for the input shaft bearing. Flanges on the housings are used to accommodate these bolts on either ends of each housing. A 3D model of a section of the DVT housing along with the dimensions is shown in figure 20. The rectangular section cut out on the side of the housing provides the braking mechanism interface with the DVT. For strength considerations of the DVT housing, the material of the housing was chosen as aluminum alloy 7075, which is the strongest grade of aluminum. The defining dimensions on the housing were constrained by the carrier design and the bearings selected. Again, the bearing catalog[19] was used as the guide in determining the necessary tolerance values. This was discussed in the previous sections. For the purpose of mounting the housing on the test stand for the proto type evaluation, feet with mounting holes

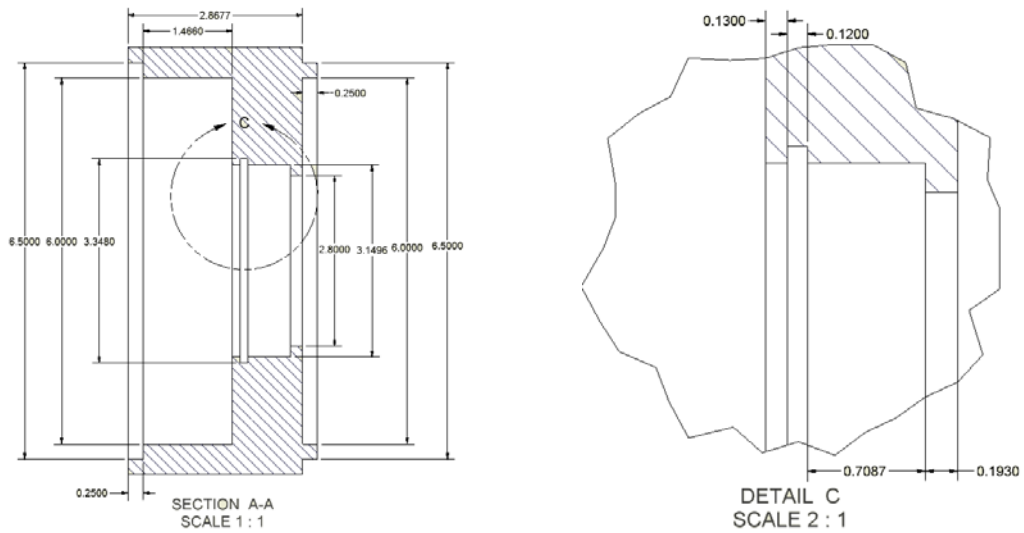
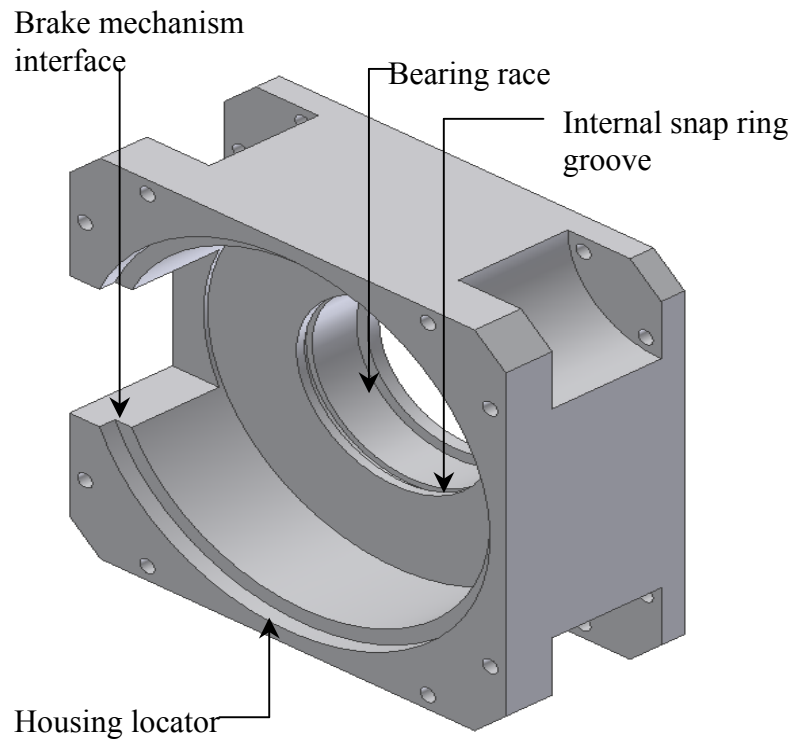


Figure 20 – DVT Housing 3D Model and Dimensions

were designed for the first and last pieces of the housing. The housing contains the lubricant, which is the synthetic automatic transmission fluid. An exploded view of the DVT housing unit is provided in the appendix.

4.5 Brake Mechanism Design

A conceptual design of the brake mechanism along with comparison of different actuation mechanisms is discussed in [12]. The DVT brake mechanism operates as a slider crank mechanism in which the stroke line of the slider is offset from the axis of rotation of the crank. This provides a compact design and offers large force amplification. A DC motor coupled with a gear head serves as the actuator for the braking mechanism.

Figure 21 shows the brake mechanism for DVT. As a part of detailing the brake mechanism, one has to establish the design requirements. In this case, the design is driven by the amount of motion the slider has to have for the band brake to fully stop the ring gear. This in turn depends upon the clearance between the band brake and the ring gear in the fully disengaged position and the motor that is selected for the design. Not to mention, the ultimate goal is to come up with a design that is compact. With this in mind, the overall size of the brake actuation mechanism was constrained to 3 inches from the top of the DVT housing. The DC motor selection was based on the brake torque requirements (*a value of 30N-m*) and also the shifting time requirement. Based on these considerations, the major dimensions of the brake mechanism are as follows.

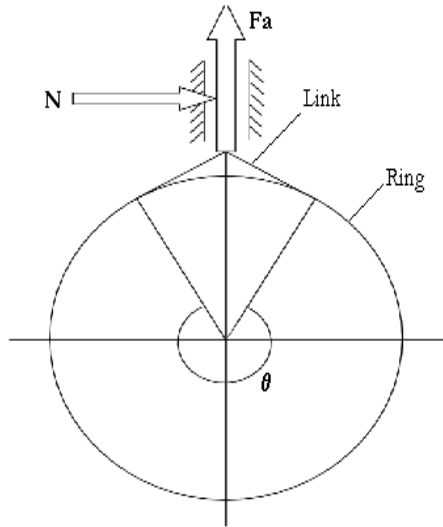


Figure 21 – Conceptual Design of the Brake Mechanism

These numbers were obtained from a dynamic simulation in Solid works by Renbin Zhou.

- ✓ Length of the crank – 0.7inches
- ✓ Length of the connecting rod – 0.7inches
- ✓ Length of the links – 0.6inches

At the initial stages of the design, hime joints were proposed for the links. The advantage of using hime joints is that, they offer length adjustment, which is very good design flexibility. Moreover, they are available commercially in a variety of sizes. But due to the size constraints imposed on the brake mechanism, hime joints could not be used. E.g. the eyes on the band brake were to be made big and wide enough to accommodate the hime joints. Another design difficulty was designing the slider. Hence, it was required to custom design the links. The

material of the links is 4140 steel. The thickness on the link was limited by the width of the slot available on the band brakes where the links attach. With custom-made links, the design was made compact. Now, the motion of the slider is not limited by the location of the connection with the links. The detailed brake mechanism for the DVT is shown in Figure 22. The slider is supported in a L-bracket that is mounted on the DVT housing with bolts. The L-bracket also acts as a support to the brake motor. The L-bracket is made of Aluminum alloy 6061. Figure 23 shows the isometric view of the L-Bracket and the brake mechanism along with the band brake and the ring gear. Two webs of $\frac{1}{4}$ inch thick were made on either sides of the bracket to offer a better support for the bracket against flexure. All the links are connected together with pins made of cold rolled steel. These pins are restrained axially using suitable retaining rings.

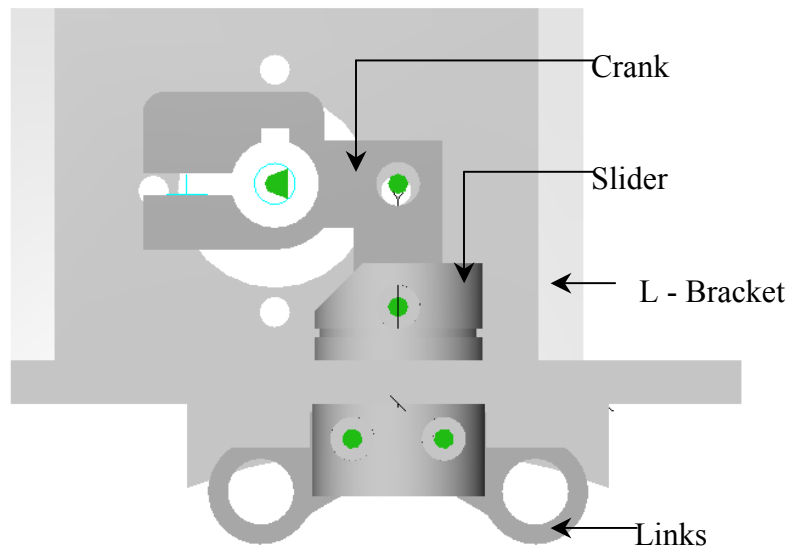


Figure 22 – DVT Brake Mechanism

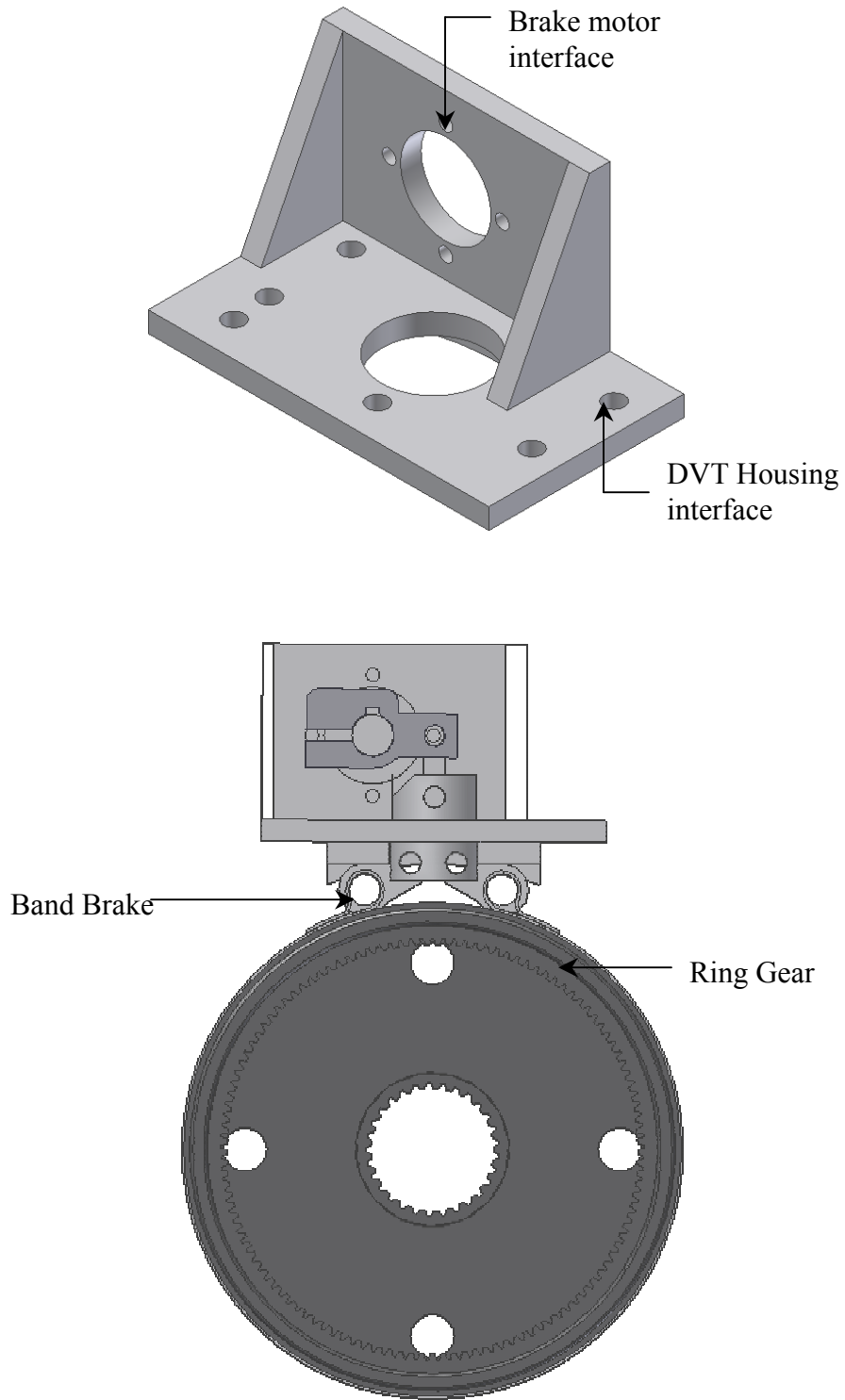


Figure 23 – L-Bracket and the Complete Brake Mechanism

Of the various brake mechanism components, the link that connects the slider to the band brake is 1/8-inch thick and hence it was decided to perform a finite element analysis of this link, to make sure it can withstand the loading that will be experienced. The vertical pulling force is around 400lbs and this value of loading is used in the analysis. Pro-Mechanica was used to do the finite element analysis. The yield stress of the material of the link is 60495psi. The Finite element model predicted a maximum von-mises stress value of approximately 14,000psi, which is well below the yield point. The loading and the constraints that were imposed on the part for the FE model is shown in Figure 24. The von mises stress contour for the link is shown in Figure 25.

A static test of the brake mechanism was performed before assembling it on to the DVT system to measure the amount of torque that can be held by the brake mechanism. Refer [12] for details on the static brake test. One manufacturing issue related with the band brake is the inability to control the distance between the eyes on the brake band and the center of the band. This resulted in the eyes of the band hitting the bottom of the L-bracket and hence the

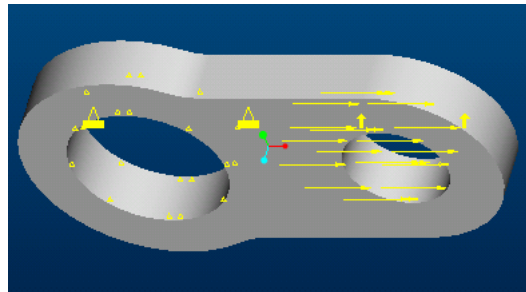


Figure 24 – Band Link Finite Element Model

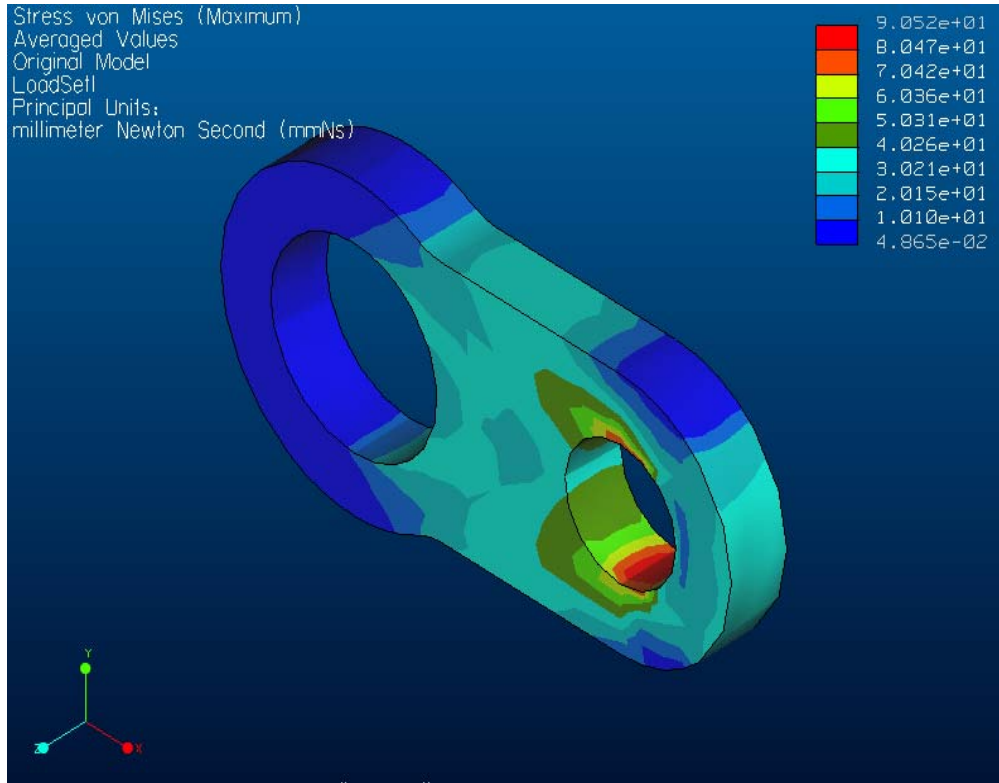


Figure 25 – Stress Results for the Band Link

band could not achieve the desired wrap angle to stop the ring gear. To solve this problem, an aluminum spacer of $\frac{1}{4}$ inch thick was designed to fit in between the L-bracket and the DVT housing.

4.6 Summary

This chapter described the detail design process of the DVT components. Finite element analysis results for the band brake links were presented. Detailed design drawings for the components were developed. The chapter ahead discusses a finite element modeling of the gear tooth, to ensure proper design.

Chapter 5

Virtual Model of the DVT in Pro/Engineer

This chapter is aimed at developing a virtual model of the discrete variable transmission in Pro/Engineer software. The goal is to determine the stresses in the gears in order to determine how much the gears could be downsized to reduce the weight of the DVT. This involves two phases. The first phase is to build a dynamic model of the three-stage DVT using the Pro-Mechanica motion. The second phase is the stress analysis of the gear teeth using Pro-Mechanica structure. The model built using Pro-Mechanica motion can be used to provide useful information about the forces at the point of contact between the gear teeth. These forces can be used in the finite element analysis of the gears, the results of which can be used as a starting point for the optimization study. The highest gear ratio of the DVT is considered for this analysis, as it transmits the highest loads.

5.1 Introduction

In the recent years, there has been a great interest in computer based modeling of mechanical systems. With the enhancement of technology, Computer Aided Design (CAD), Computer Aided manufacturing (CAM) and Computer Aided Engineering (CAE) can be found in almost all industries

involved in design and manufacturing. Computers are capable of performing mass computations very quickly and efficiently. Due to the advances in CAD, it is now possible to realize designs, which were previously only imagined.

CAD software has revolutionized the mechanical design process. Almost anything and everything that we see in the real world is built digitally with the click of the mouse. A fast-paced design environment requires frequent changes in the design and accurate representation, which is provided by CAD software. The parts developed using CAD software can be used to get model information like mass properties, coordinate geometry, volume etc., from the model database. Models developed in CAD packages can be exchanged over the internet and so engineers can exchange their design ideas more effectively and easily. Parametric modeling is another powerful capability of most of most CAD software. This allows the designer to specify design parameters and their relation with the other model dimensions. As a result, part modifications can retain the original design intent, with all part dimensions updating automatically with any dimensional change.

Three-dimensional CAD software offers certain advantages over two-dimensional modeling. Apart from providing a good visual representation of the parts, parts modeled in 3D can be assembled in the software itself and any errors in the design or interference with the other parts can be identified. Creating drawings in 3D allows the different drawing views to be generated automatically from the 3D model of the part. Any changes to the part are reflected in the

drawing, thus making the revision of the drawings much easier. This helps saving the labor cost and time associated with these tasks. Complex mechanisms involving large numbers of components and connections can be modeled and the motion of the system can be simulated using specialized software. Moreover the 3D models can be used for rapid prototyping and tooling and to perform finite element analysis to enhance the design. In the marketing illustrations for sales brochures and instructional bulletins, digital mock-ups of three models are used. These advantages of the CAD systems make them extremely suitable for industrial and research environments.

Some of the most common CAD packages are Pro/Engineer, AutoDesk Inventor, Solid Works, Unigraphics, Catia and AutoCAD. Each of these packages is suited for a variety of applications. For the dynamic analysis of the DVT system, which involves applying the loads and drivers, Pro/Engineer is used. The advantage of using Pro/Engineer is that it has both CAD and CAE tools that support a wide range of analysis capabilities including dynamic analysis, which is available in very few other software packages.

5.2 CAD Model Representation of DVT Components

CAD model representation of the DVT is the process of modeling the DVT components and assembling them together with the help of suitable constraints that specify the motion of the component in the actual system. An example is a four bar linkage in which the different links are connected to each

other with pin (revolute) joints. Pro/Engineer assembly is driven by the purpose of the assembly. If the assembly has to be used for a motion analysis or an optimization study, then care must be taken to build the assembly in such a way that it can be run with the specified loads and constraints. On the other hand, if the assembly is to be used for the purpose of checking the design or for the final component visualization, the different components can be packaged with respect to the other. In the process of building the prototype of the DVT, AutoDesk Inventor 6.0 was used for the 3D modeling and to generate the drawing blue prints. A detailed list of the components along with their drawings can be found in the appendix. Since AutoDesk Inventor is purely a 3D modeling package that does not support any sort of analysis capabilities, Pro/Engineer was used to perform this task.

The initial motive of this work was to develop the Pro/Engineer model with the actual gears rather than representing them using cylindrical surfaces. The advantage of doing this would be to have the motion analysis directly import the loads to the structural model. This could be accomplished in Pro-Mechanica motion using a contact analysis. Since the model here deals with three sets of planetary gear trains, the number of contact surfaces is too high for a current desktop computer. Hence the alternative to this, the representation of the gears by the pitch surface, was chosen. Each gear is represented by its pitch circle diameter, which is the diameter at which the gear teeth come in contact with each other. As discussed before, in the case of the DVT, because of the use of non-

standard gears, the pitch circle diameters of the gears do not come in contact. Instead each pair of gear has its operating center distance and operating pressure angle, which can be calculated using the relations below. In the case of external spur or helical gears the operating pitch diameters are,

$$D^1 = \frac{2 * C^1}{m_g + 1} \text{ (Pinion Member)} \quad (5.1)$$

$$D^1 = \frac{2 * C^1 * m_g}{m_g + 1} \text{ (Gear Member)} \quad (5.2)$$

And for internal spur and helical gears,

$$D^1 = \frac{2 * C^1}{m_g - 1} \text{ (Pinion Member)} \quad (5.3)$$

$$D^1 = \frac{2 * C^1 * m_g}{m_g - 1} \text{ (Gear Member)} \quad (5.4)$$

The other gear train components viz., splines, bearings are not modeled for this analysis. The primary focus will be on doing the stress analysis for the gears.

The Pro/Engineer assembly of the DVT is shown in Figure 26. At this point building the gear train components is merely couple of extrusions. One important point to be noted is the coordinate system and the orientation of the components with respect to the world coordinate system. All rotational elements of the gear train should have their z-axis in the same direction. Else the rotational inertia may not be incorporated correctly in the analysis. Since the sun gear and the planet carrier have a common rotational axis, a datum axis was created in the

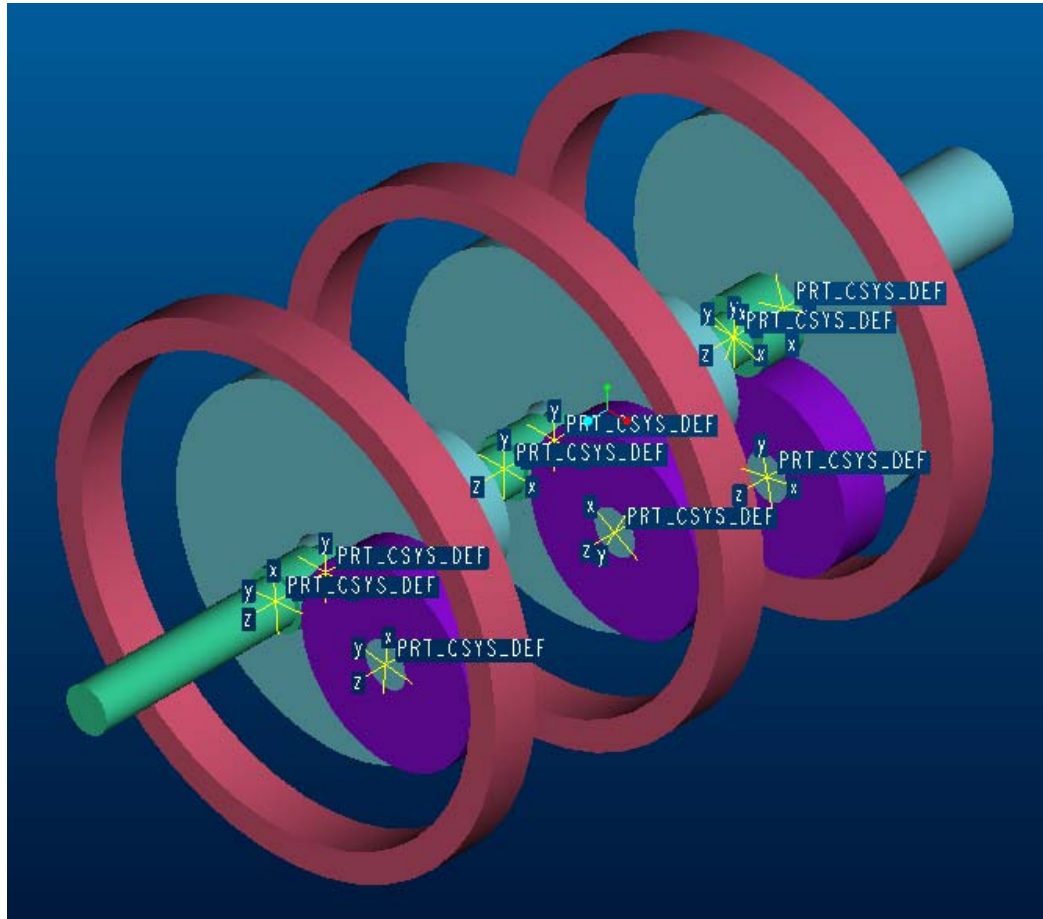


Figure 26 – Pro-Engineer Model of the Three-Stage DVT

Pro/Engineer assembly and all the components were constrained to be pin jointed with respect to this common axis. If the housings are modeled, the centerline of the housing can be used to constrain the components. Another issue to be addressed in the assembly is the redundancy of constraints. An over-constrained system cannot be used for the motion analysis and care must be taken to avoid this situation. For example, in the DVT system, the carrier-ring configuration caused the problem of constraint redundancy and this was overcome by making a carrier-ring sub-assembly.

5.3 Pro-Mechanica Motion Analysis

Having assembled the DVT system, Pro-Mechanica can be invoked to perform the motion analysis. The purpose of the motion analysis is to develop a model of the DVT so that it can be used to study the dynamics of the system. For the current model, only the steady state was examined. Primary data that was obtained from the analysis was the gear pair contact forces in the first gear. Apart from this, the model served to verify the analytical model described in chapter 3. This model can be used as the basis for modeling the gear shifting, which can be done by creating a feedback loop between the input and the output and make the gear shift dependent on the load. The appropriate material properties are assigned to each component and gear properties, such as the pressure angle and the type of gear, are assigned to the gear surfaces. The built-in gear properties in Pro-Mechanica allow the designer to choose from a wide variety of gears. Pro-

Mechanica treats the components of a mechanism as separate “*bodies*”. It is a good design practice to group components that do not move relative to each other, which saves the analysis time. These steps were initially done to make sure that there were no modeling errors.

The type of dynamic model that is built here is an *inverse dynamic model*. In an inverse dynamic model, a kinematic driver dictates the motion of the model. Loads are then applied to the model, which could be a fixed or variable torque or force. As the mechanism runs through its motion, Pro-Mechanica calculates the amount of torque that the driver must supply in order for the prescribed motion to take place. This kind of an analysis plays a vital role in the conceptual design stage of a project, where it can be used to size the driver and the different components in the mechanism.

Pro-Mechanica has built in position, velocity and acceleration drivers but none of these provide the capability of control the torque input to the system. It could be possible to build a custom load that takes care of the torque-speed characteristics of the motor. In that case a feedback loop must be used so that the driver supplies the required torque input based on the output. This could be done by using C or FORTRAN programming routines. Since the data for the stress analysis can be obtained from an inverse dynamic model, the former approach was not implemented. However to study the behavior of the system in the transient state, for example when there is a gear change, this approach could be used.

5.3.1 Single-stage Planetary Gear Train

To validate the results of the Pro-Mechanica analysis, a single stage planetary gear train is considered. Input to the system is the sun gear, which is driven with a constant acceleration of 20rad/sec^2 (final speed of 200rad/sec). No load is applied to the system. The DVT is held in a particular gear by holding the ring gear, which is done in Pro-Mechanica by applying a “zero-position driver”. The analytical results are shown below and the graphical results from Pro-Mechanica are shown in Figure 27. It can be seen that the results well agree each other.

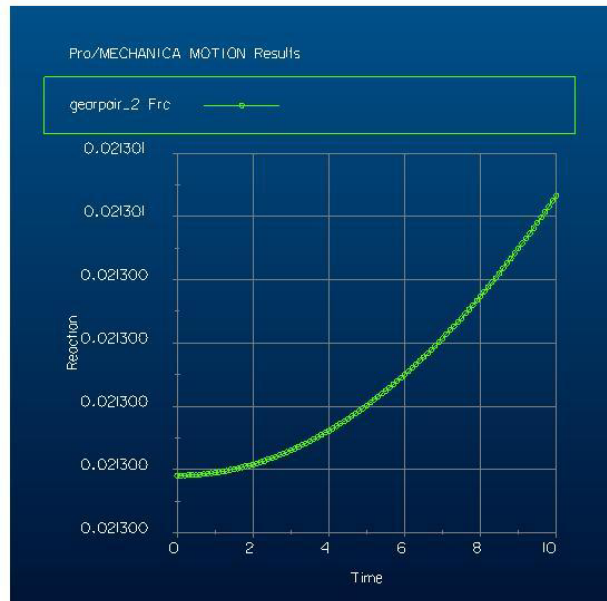
Analytical Results for a Single Stage Planetary Gear

Properties of the gear train members

$$\begin{aligned} J_S &:= 6.719 \cdot 10^{-06} && \text{Kg} - m^2 \\ r_S &:= 0.0081 && m \\ m_P &:= 0.212 && \text{Kg} \\ J_P &:= 8.085 \cdot 10^{-05} && \text{Kg} - m^2 \\ J_C &:= 4.821 \cdot 10^{-04} && \text{Kg} - m^2 \\ r_C &:= 0.034 && m \\ r_P &:= 0.027 && m \\ J_R &:= 1.450e^{-03} && \text{Kg} - m^2 \\ T_R &:= 122 \\ T_S &:= 16 \\ T_P &:= 53 \\ \dot{\omega}_s &= 20 && \text{rad} \cdot \text{sec}^{-2} \end{aligned}$$

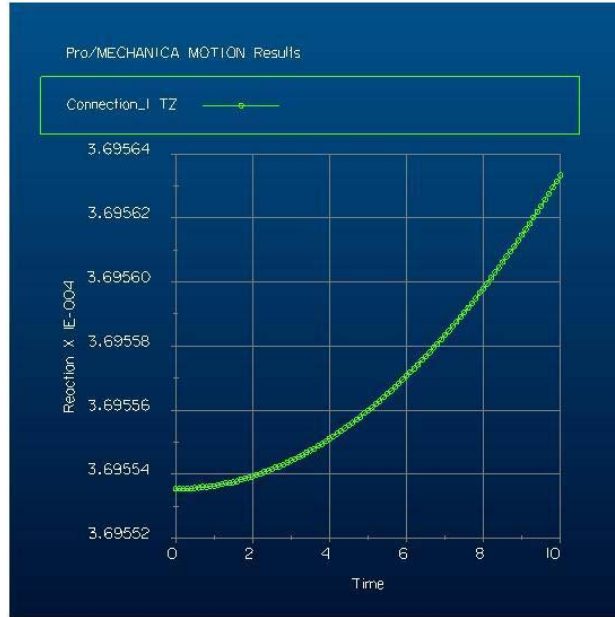


(a) – Force at the Sun-Planet Mesh

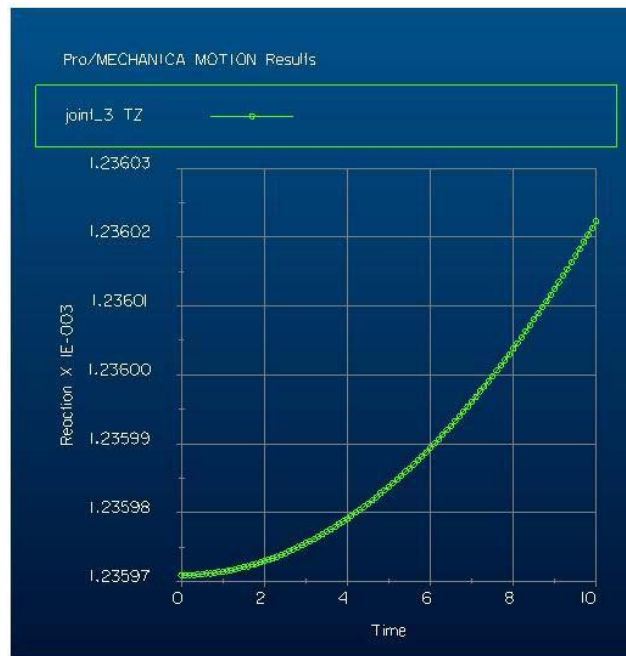


(b) – Force at the Planet-Ring Mesh

Figure 27 – Pro-Mechanica Results for a Single Planetary Gear Train



(c) – Input Torque



(d) – Brake Torque

Figure 27 Continued

Contact force at the Sun-Planet mesh

$$a_1 := \frac{T_S}{T_S + T_R}$$

$$a_2 := \frac{T_R}{T_S + T_R}$$

$$b_1 := \frac{[T_S - a_1 \cdot (T_S + T_P)]}{T_P}$$

$$b_2 := -a_2 \cdot \frac{(T_S + T_P)}{T_P}$$

$$F_{PST} := \left[\frac{[(m_P \cdot r_C^2 \cdot a_1) + (J_C \cdot a_1)]}{(2 \cdot r_C)} + \frac{(J_P \cdot b_1)}{(2 \cdot r_P)} \right] \cdot \dot{\omega}_s$$

$$F_{PST} = 0.029 \quad N$$

$$F_{PS} := \frac{F_{PST}}{\cos(20deg)}$$

$$F_{PS} = 0.031 \quad N$$

Force at the Ring-Planet mesh

$$F_{RPT} := \left[\frac{[(m_P \cdot r_C^2 \cdot a_1) + (J_C \cdot a_1)]}{(2 \cdot r_C)} - \frac{(J_P \cdot b_1)}{(2 \cdot r_P)} \right] \cdot \dot{\omega}_s$$

$$F_{RPT} = 0.02 \quad N$$

$$F_{RP} := \frac{F_{RPT}}{\cos(20deg)}$$

$$F_{RP} = 0.022 \quad N$$

Input and Braking Torque results

$$\begin{aligned}\tau_S &:= (F_{PST} \cdot r_S) + (J_S \cdot \ddot{\omega}_s) \\ \tau_S &= 3.718 \times 10^{-4} \quad N - m \\ \tau_B &:= F_{RPT} \cdot \frac{0.123}{2} \\ \tau_B &= 1.247 \times 10^{-3} \quad N - m\end{aligned}$$

5.3.2 Three-stage Planetary Gear Train

With the Pro-Mechanica results verified for a single stage planetary gear train, it is reasonable to extend it to the three-stage DVT. Each gear ratio is obtained by holding the ring gear of the corresponding stage. Again it should be noted that this is a steady state analysis of the system. The gear shifting and other non-linearities such as backlash, friction etc., associated with the system are ignored. Results that will be obtained from the model are the brake holding torques for each gear, the gear teeth contact forces and the motor torque profile.

Since the system does not include a final reduction of 200:1, the load that will be applied to the DVT output will be a scaled value of the actual shoulder joint torque. Referring to Figure 28, the following formula is used to calculate the joint torque of the manipulator arm. This torque will be applied at the output of the DVT system in the Pro-Mechanica model. The arm is assumed to move from

$$T = (Mp + \frac{1}{3}Ma)l^2 \ddot{\theta} + (Mp + \frac{1}{2}Ma)l.g.\sin \theta \quad (5.5)$$

a zero degree position (which is the straight down position) to a 180-degree

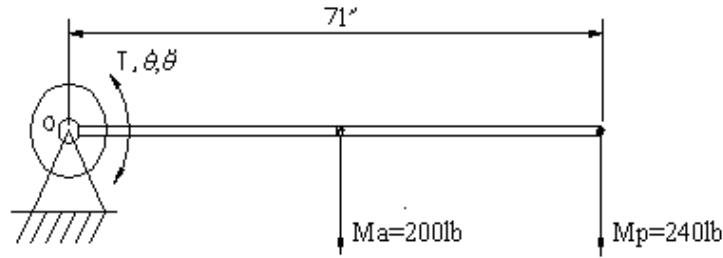


Figure 28 – Arm Configuration for Prototype Evaluation

position (the straight up position), which is the pitch up maneuver. It can be seen from the above equation that the joint torque will be a maximum at the point where $\theta=90$ degrees. At this position the arm moves with a constant velocity and the acceleration is zero. Therefore,

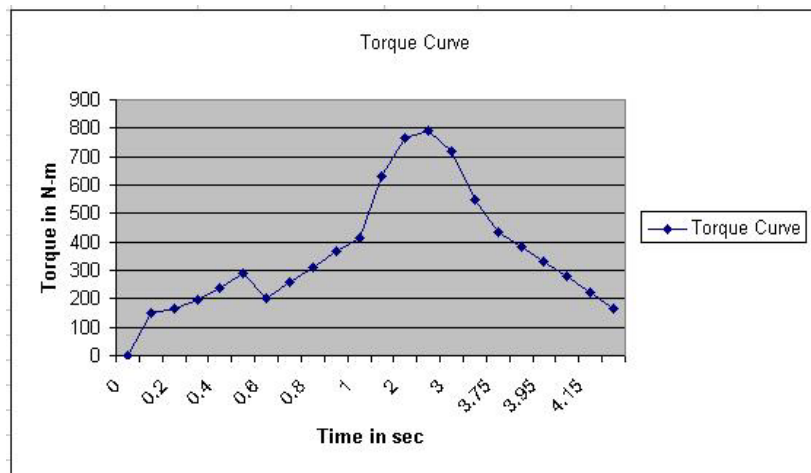
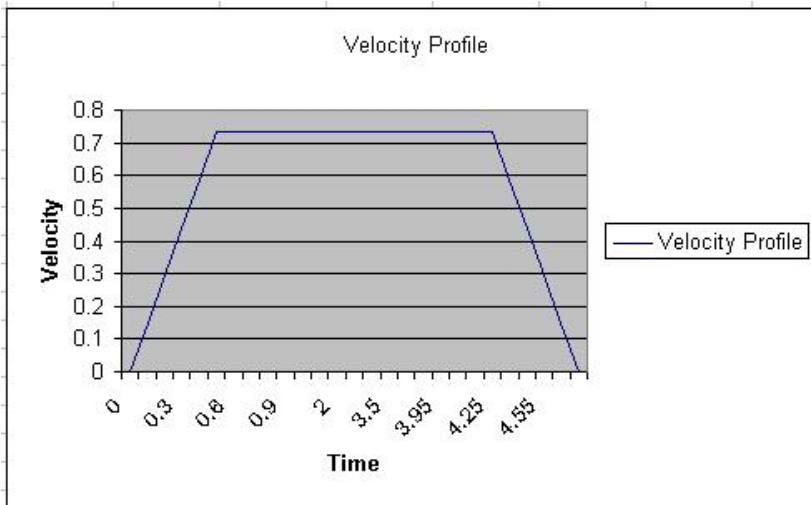
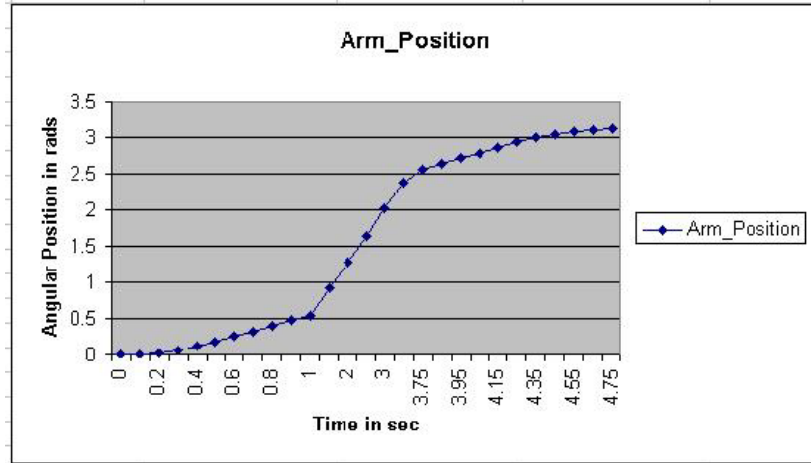
$$T = (Mp + \frac{1}{2}Ma)l.g \quad (5.6)$$

The numbers indicated in the above figure are obtained from the baseline requirements[†]. Two cases are considered here.

Case 1

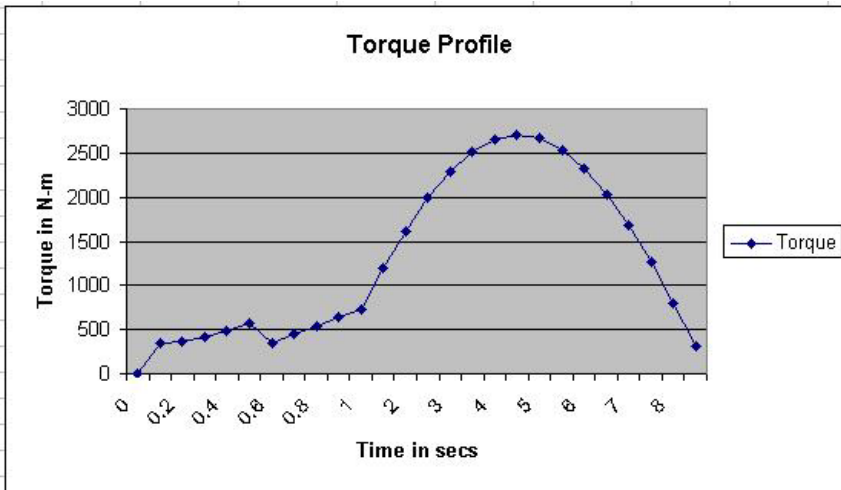
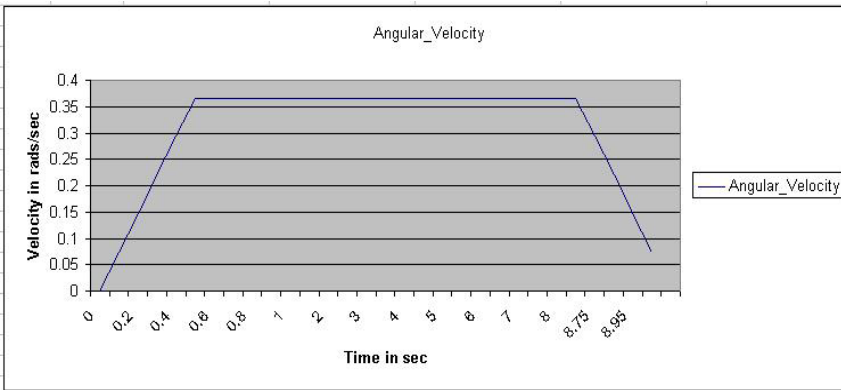
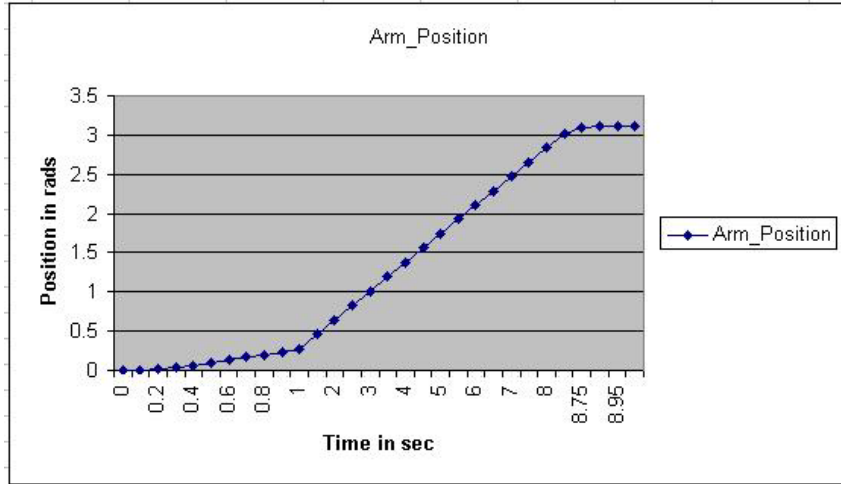
For this case, the joint torque is calculated for a no payload condition. As can be seen from the above equations, the joint torque is a function of the arm position and arm acceleration. An acceleration of 1.466 rad/sec^2 (*obtained from the baseline requirements*) will be used here. The arm is assumed to move continuously from a zero degree position to 180 degrees. The profiles are shown in Figure 29 (a).

[†] Robotics Laboratory Internal Document



(a) Case 1

Figure 29 – Position, Velocity and Acceleration Profiles



(b) Case 2

Figure 29 Continued

Case 2

Here the payload is considered at the end of the arm and the acceleration value of the arm is 0.733 rad/sec^2 . The inertial properties of the arm and the payload weight are indicated in the Figure 28. The following is the formula that was used to calculate the position values for the two cases. Figure 29 (b) gives the position,

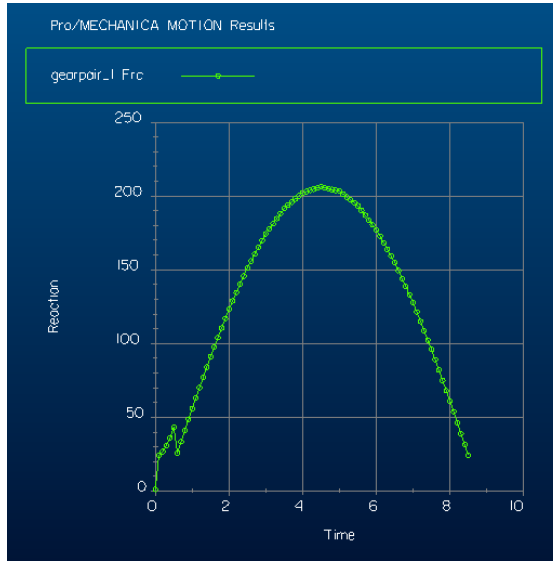
$$\theta = \theta_o.t + \frac{1}{2}.\alpha.t^2 \quad (5.7)$$

velocity, and torque profiles with respect to time this case.

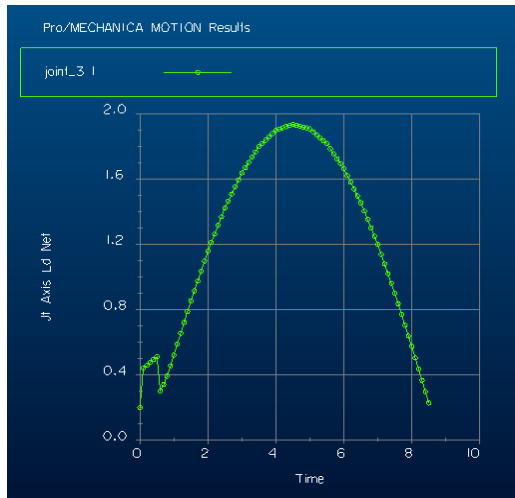
The torque profiles shown in the above figures are scaled down by a value of 200 (*because a final reduction of 200:1 is not considered here*) and used as the load torque for the Pro-Mechanica model, which is the input to the model. The model can be queried for the input (sun gear) torque, brake torque and the gear teeth forces. The results of the model are shown in Figure 30.

5.4 Gear Tooth Stress Analysis

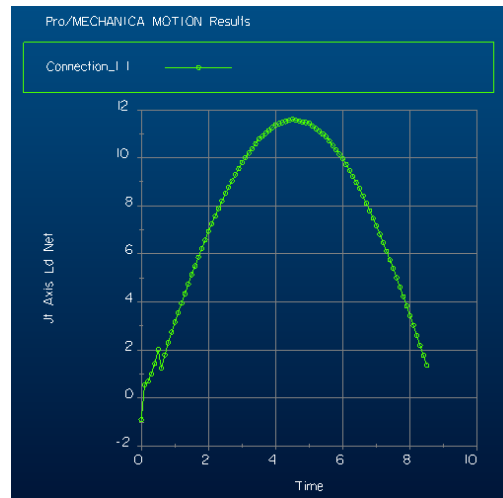
When designing gears, as is the case with any component, the designer has to make sure that the gears can handle the loads to which it will be subjected to without any interruption or degradation for a determined period of time. Gear tooth stress analysis is an important part of the design process. Therefore this section is devoted to the process of verifying the strength of the DVT gear tooth using finite element results from Pro-Mechanica. Before this, the common modes of failures for the gear tooth are examined. This would help the designer to better



(a) Gear Teeth Contact Forces (Sun-Planet Mesh in N)



(b) Motor Torque (N-m)



(c) Brake Torque (N-m)

Figure 30 – Pro-Mechanica Results for a Three-Stage Planetary

examine the results from the software package.

5.4.1 Gear Tooth Failure Modes

This section describes the most common failure modes for the gear tooth. Gear tooth failures can be categorized into different classes viz., wear, scoring, interference, surface fatigue and fracture. Wear of the tooth occurs when the oil film between the two gear teeth is not sufficient to prevent the surface-to-surface contact. Wear of the tooth is affected by many factors such as the thickness of the lubricant film, relative surface roughness of the tooth flanks and the amount of contamination of the lubricant. Gear failure due to interference occurs when the tip of one gear contacts mate below the point at which the involute exists. The reasons for interference may be tight center distances and manufacturing errors. Due to the nature of operation of the gears, the gear tooth surfaces are subjected to the repeated application and removal of the load. This causes fatigue. When the resulting fatigue exceeds the fatigue capacity of the material, the gears fail. The modes of failures associated with surface fatigue are various degrees of pitting and spalling. All these failures occur over a period of time and there is a significant time between the failure initiation and complete loss of the gear. But gear fracture is more of an instantaneous mode of failure. The result is reduced efficiency of the power transmitted. Bending fatigue is a type of failure that originates in the fillet area of the tooth at the critical section near the tangency point between the involute profile and the fillet. This type of failure is a result of

stresses caused due to the loading that is above the level of allowable stress. Other types of gear failures could be process related. This might be in the form of errors in manufacturing, or improper heat treatment process that result in residual stresses.

5.4.2 Finite Element Modeling of the Gear Teeth

The motion analysis of the DVT system in Pro-Mechanica was used to determine the force between the gear teeth at the point of contact. This force is now used to predict the stress distribution along the tooth profile and the tooth deflection. The analysis is performed on the gear tooth of the final stage planetary gear train, as this provides the highest torque amplification. Results of the stress analysis can be very useful to show by what degree the system is over designed and also estimate possible weight reduction. For a non-standard gear tooth, the stress values can be used to determine the fillet radius that will result in lower stress concentrations.

Figure 31 shows the Pro-Mechanica model of a spur gear tooth along with the loads and constraints. The load was applied over the entire involute profile. This should not significantly affect the final result of the analysis because this load is at a substantial distance away from the location of peak stress and hence the local effects of the load will be negligible. The tooth was modeled to the extent that the constraints on the model do not influence the stress results. It should also be noted here that a contact ratio (*which is the number of teeth in*

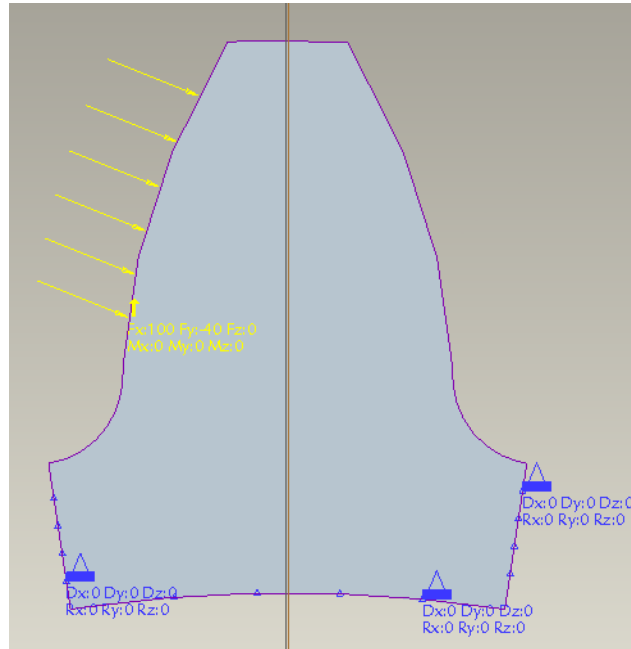
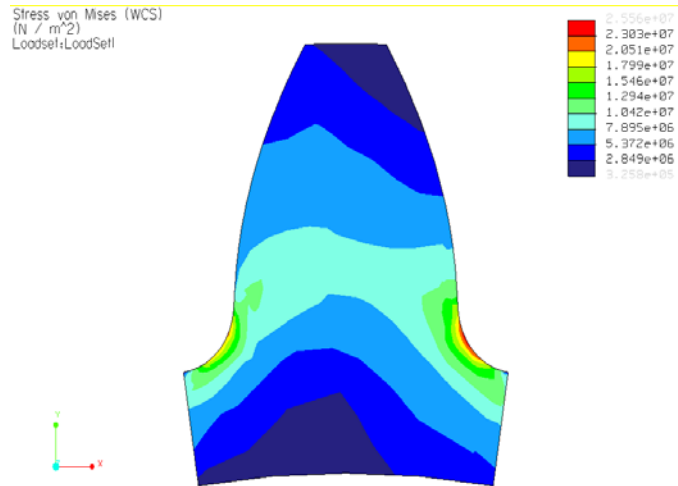
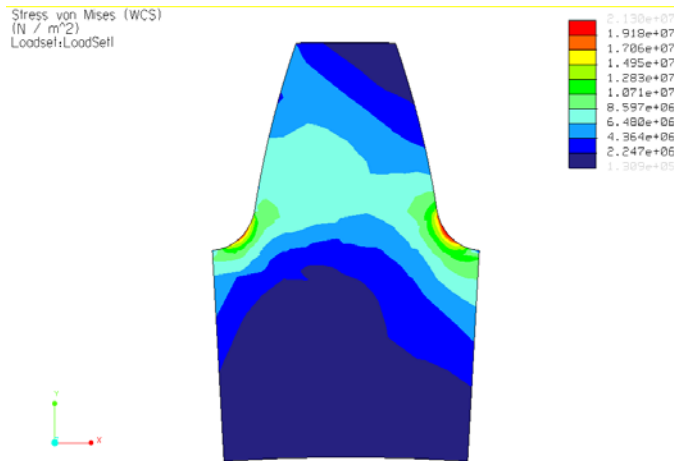


Figure 31 – Loads and Constraints on a Single Spur Gear Tooth

contact at each mesh) of 1 is assumed. This means that one gear tooth at each interface takes the entire load. In the actual case the contact ratio is more than 1. So the worst-case loading conditions are assumed. A plane stress model is used in this case with a shell thickness of 0.5 inches, which is the face width of the gears. The stress contour that was obtained from the software is shown in Figure 32. The stress plot shown here is the Von Mises stress, which is the most conservative estimate of the result. As expected the maximum stresses were found along the two fillets, which are the regions of compressive and tensile stresses. From the stress numbers, it can be seen that the maximum stress (23.03Mpa) in the results are well below the yield point (472.3Mpa) of the material of the gear. The sun, planet and the ring gears have different tooth



(a) Stress Plot for the Sun Gear



(b) Stress Plot for the Planet Gear

Figure 32 – Gear Teeth Stress Results

geometries. Hence, the same analysis was performed on the planet gear tooth and the corresponding stress plots are shown in Figure 32. The tooth profile of the ring gear tooth could not be modeled precisely in Pro-Engineer. The stress results of the planet and sun gear teeth can be used to state that the stresses on the ring gears will well be within the safe limits.

5.5 Summary

This chapter developed a Pro-Mechanica model of the DVT system. The model was used to get gear teeth contact forces for a loading case and these forces were used to perform a finite element stress analysis of the gear teeth.

6.1 Conclusions

Till this point of the report, the design process of the DVT was discussed. As mentioned earlier, the manufacturing of the DVT was contracted to Ann Arbor Gear Technologies. Since the DVT is an assembly of nearly 100 components, the tolerances to be maintained are very high. This manufacturer is well known for their gear manufacturing capabilities in the automotive industry. Detailed design drawings, made using AutoDesk Inventor 6.0, for all the components were provided for manufacturing. The manufacturing took around 3-4 months and a three-member team, comprising Dr. Bill Hamel, the author and Kelley P. Brown, from UT went to the manufacturers facility to assemble the transmission system. The individual components and the total assembly of the DVT system are shown in the Figure 33. The brake mechanism was simple enough to be fabricated in the machine shop at University of Tennessee, Knoxville.

Initial test[‡] plan for the DVT system was to build a mock up arm that matches the inertia properties indicated in figure. This involved designing the final reduction of a 200:1.

[‡] The DVT test and controls was performed by Dr. Sewoong Kim and Renbin Zhou

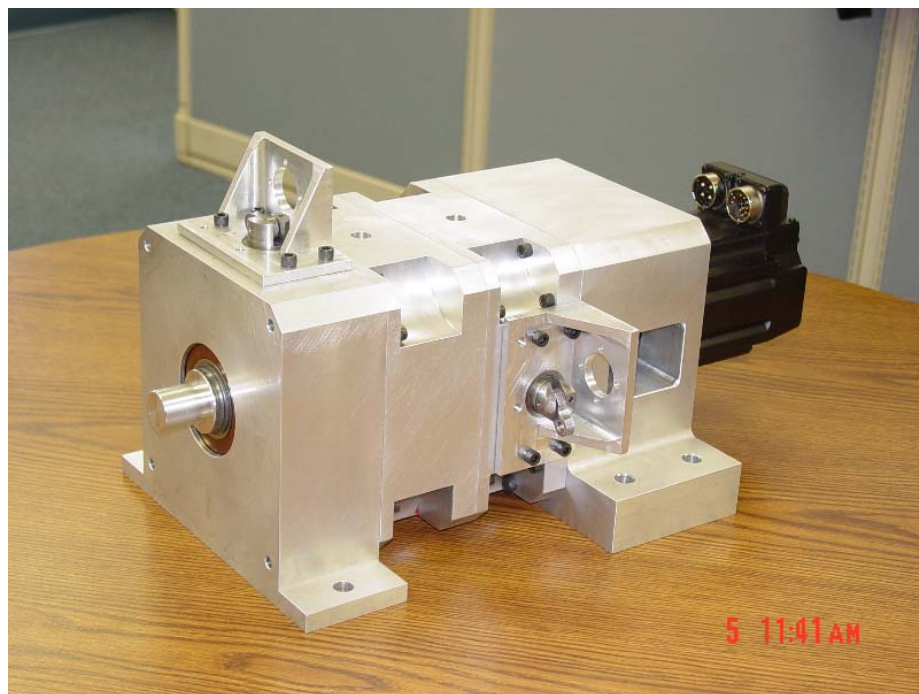


Figure 33 – DVT Components and Assembly

Considering the safety as well as time issues with building the arm, the focus was diverted towards testing the functionality of the DVT using a dynamometer that could emulate the loading characteristics of the robotic arm. The dynamometer that was used for the test is an eddy current, water-cooled absorption dynamometer. The dynamometer generated the desired torque profile, based on the input voltage applied to it. Figure 34 shows the test set up. The results of the test were encouraging. The transmission system built was able to handle the loading conditions and the gears were able to shift with out any mechanical failure of components. Figure 35 shows a sample test result to show the operation of the DVT system. The graph shown in the figure shows the gear shifting. This was a result generated by applying the full load, (*arm payload and inertia*) to the DVT.



Figure 34 – DVT Test Setup

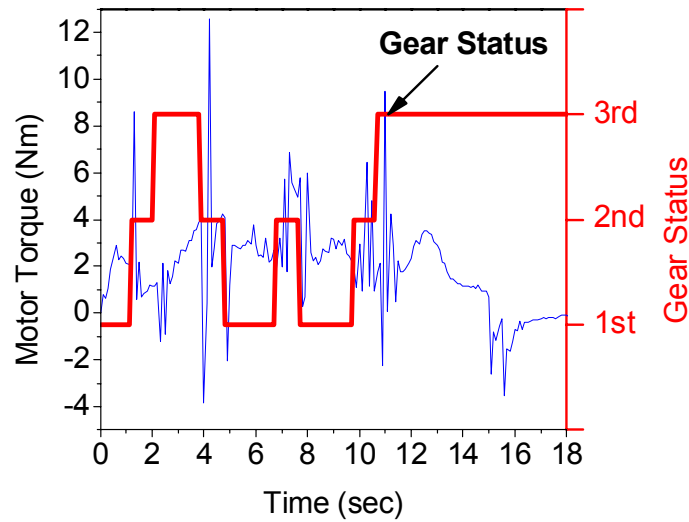


Figure 35 – DVT Sample Test Result

6.2 Future Work

The use of a three-speed transmission system along with a DC motor is feasible for robotic actuator applications involving heavy payload. The different tests conducted, verify this idea. Hence future research should be focused towards designing a more compact DVT, which comes to optimization of the present design. For DVT to be implemented commercially, it has to satisfy the size and weight limitations. The overall envelope of the DVT is determined by the cross sectional dimensions of the housing, which in turn depends on the gear sizes, bearings and the gear shifting mechanism used. The components of the band brake mechanism increase the DVT envelope by a great extent. Hence research should be focused in this area. When looking at optimizing the system, the first possibility to look at is the DVT configuration. A two stage DVT can

reduce the overall length to a great extent. The design configurations are limited if we look at achieving three different speed ratios from two planetary gear sets. Use of clutches becomes necessary with this kind of configuration. This might introduce some design complexities. A possible configuration with two planetary gear trains is shown in Figure 36. This design is mostly the same as the current design, except for a clutch mechanism that must be used to change the power flow from one stage to the other. In this case, the clutch mechanism should be able to shift the power flow from the carrier-ring and carrier-carrier. With the same gears as the present design, the reductions possible for the new design are shown in the appendix. The carriers of the system need some modifications and so do the ring gears.

With the three-stage DVT, one can look at possibilities of optimizing the ratios, using a different motor that has a lower speed and having a reasonable

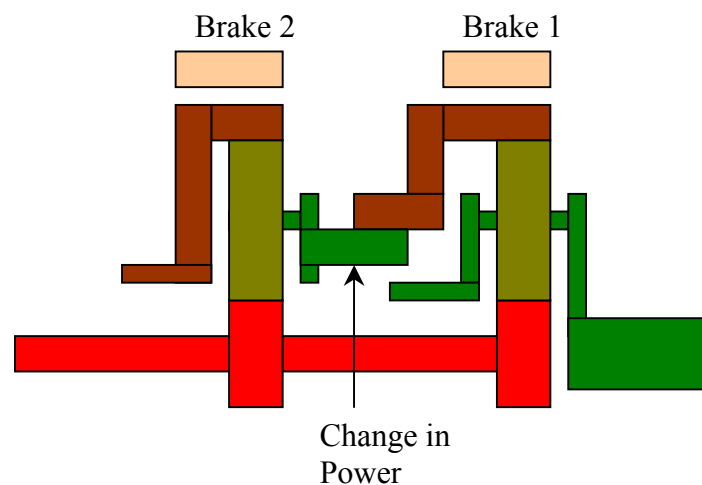


Figure 36 – Two-Stage DVT

power output. Stress analysis results on the sun and planet gear teeth show that a face width of 0.25 inches can be used for the gears. This can further reduce the length of the input shaft and also the distance between two stages of the gear train. Hence, the length of the DVT could be reduced to some extent along with some weight reductions. Different options for the brake mechanism were discussed in [12]. Using that information and the test results one can look at an alternate mechanism that can generate the required brake torque.

Bibliography

- [1] T. B. Sheridan, "Telerobotics". International Federation of Automatic Control, Vol. 25, No.4. pp. 487-507, 1989.
- [2] Phillip John McKerrow. "Introduction to Robotics", Addison-Wesley Publishing Company, Singapore 1991
- [3] <http://www.robotics.utexas.edu/urpr/research> University of Texas, Austin Research web page.
- [4] Frank Daerden, Dirk Lefeber, Björn Verrelst, Ronald Van Ham. "Pleated Pneumatic Artificial Muscles: Compliant Robotic Actuators" Vrije Universiteit Brussels. Department of Mechanical Engineering / Multibody Mechanics Group.
- [5] <http://www.ai.mit.edu/projects/cog/publications.html>. Massachusetts Institute of Technology research link.
- [6] Murat Cenk Cavusoglu, Alana Sherman, Frank Tendick. "Bilateral Controller Design for Telemanipulation in Soft Environments". In the proceedings of the IEEE International Conference on Robotics and Automation, Seoul, Korea, 2001
- [7] <http://osl-www.colorado.edu/Research/haptic/hapticInterface.shtml> Haptic Interface research at the University of Colorado, Boulder
- [8] Danny Grant, Vincent Hayward. "Constrained force control of Shape Memory Alloy Actuators". Proceedings of the IEEE International Conference on Robotics and Automation April 2000.
- [9] <http://www.robotbooks.com/robot-insects.htm> An online resource for Robotics.
- [10] T.C.Widner. "Analysis Of Transmission-Based Robotic Servo Actuator Concept" Ph.D. Dissertation, Mechanical Engineering, The University of Tennessee, Knoxville, 1999
- [11] T.C. Widner and W.R. Hamel. "Fundamental Control Concepts for Implementation of Transmission-Based Actuators in Robotics and Automation". Proceedings of the IEEE International Conference on Robotics and Automation. Leuven, Belgium 1998.
- [12] Kalyana B. Ganti. "Analysis and Design of a Gear Shifting Mechanism for Transmission-Based Actuators" Masters Thesis, MABE Department. University of Tennessee, Knoxville.
- [13] Rattan S.S., "Theory of Machines", New Delhi, India. Tata McGraw-Hill Publishing Company Ltd., 1998.
- [14] Darle W. Dudley. "Gear Handbook". Massachusetts, USA. McGraw-Hill Book Company. 1962.

- [15] Hamilton H. Mabie, Charles F. Reinholtz. “Mechanisms and Dynamics of Machinery”, New York, USA. John Wiley and Sons. 1987.
- [16] Aaron D. Deutschman, Walter J. Michels and Charles E. Wilson. “Machine Design – Theory and Practice”. Macmillan Publishing Co., Inc. New York.1975.
- [17] Society of Automotive Engineers Inc., “Involute Splines and Inspection”. Warrendale, PA. 1970.
- [18] Charles E. Wilson. “Computer Integrated Machine Design”. Prentice Hall. 1997.
- [19] “Torrington Service Catalog”. Torrington Fafnir Kilian. 2001.
- [20] Arcon Ring and Specialty Corporation. Retaining rings product catalog.
- [21] Herbert H. Alvord. “Manual of Applied Machinery Design”. University of Michigan, Ann Arbor.

Appendix

Gear data for the DVT gears

Sun Gear - 1

Feb 01 03 08:46p GEORGE BOWERS 765 349 9828 p. 2

GEAR TECHNOLOGY APPLIED, INC.
3540 WOODLAND POINT
MARTINSVILLE, IN 46151-8087

PART NUMBER P-1 & P-2
 PART NAME SUN 16 T ORIGINATOR G.L. BOWERS
 MODEL DRAGONAL TRANSMISSION
 DATE 1-29-2003 APPROVAL LB

EXTERNAL INVOLUTE SPUR GEAR DATA

NUMBER OF TEETH	<u>16</u>
DIAMETRAL PITCH (MODULE 1m ENGLISH 25.4)	<u>25.4</u>
PRESSURE ANGLE	<u>20°</u>
OUTSIDE DIAMETER	<u>.732 1.728</u>
TIP CHAMFER DIAMETER	<u>.728</u> MIN
ACTIVE PROFILE DIAMETER	<u>.601</u>
ROOT DIAMETER	<u>.558 1.553</u>
ROOT FILLET RADIUS <u>FILL</u>	<u>.019</u> MIN
CIRCULAR TOOTH THICKNESS	<u>.0703 1.0695</u>
LEAD TOLERANCE ACROSS 80% FACE WIDTH <u>LESS</u> END EDGE CHAF. / BREAK BOTH SIDES	<u>+ .0003 1.0003</u> AVG
MIN. MATERIAL OUTSIDE THE 80% LEAD VARIATION	<u>.0005</u> MAX
LEAD CROWN	<u>.0002</u> MAX
LEAD HOLLOW	<u>.0002</u> MAX
DEBURR EDGES OF GEAR TEETH	<u>.015</u> MAX

REFERENCE DATA

PITCH DIAMETER	<u>.62992</u>
BASE CIRCLE DIAMETER	<u>.59193</u>
BASE PITCH	<u>.11623</u>
MEASUREMENT OVER TWO <u>.068</u> DIAMETER PINS	<u>.7409 1.7393</u>
CENTER DISTANCE, OPERATING	<u>1.3750</u>
BACKLASH, OPERATING	<u>.0035 1.0018</u>
DESIGNED TO MATE WITH PART NUMBER	<u>53T PLANET INPUT</u>

Planet Gear - 1

Feb 01 03 08:46p GEORGE BOWERS 765 349 9828 p.4

GEAR TECHNOLOGY APPLIED, INC.
3540 WOODLAND POINT
MARTINSVILLE, IN 46151-8087

PART NUMBER P-18P-2
 PART NAME PLANET PINION SPT ORIGINATOR G.L. BOWERS
 MODEL PLANETARY TRANSMISSION
 DATE 1-29-2003 APPROVAL GB

EXTERNAL INVOLUTE SPUR GEAR DATA

NUMBER OF TEETH 53
 DIAMETRAL PITCH (MODULE 1 METRIC MOD) 25.4
 PRESSURE ANGLE 20°
 OUTSIDE DIAMETER 2.165 12.161
 TIP CHAMFER DIAMETER 2.161 MIN
 ACTIVE PROFILE DIAMETER 2.048
 ROOT DIAMETER 1.998 1.993
 ROOT FILLET RADIUS FULL019 MIN
 CIRCULAR TOOTH THICKNESS0643 1.0635
 LEAD TOLERANCE ACROSS 80% FACE WIDTH LESS + .0003 1.0003 AVG BOTH SIDES
 LEAD VARIATION0005 MAX
 LEAD CROWN0004 MAX.
 LEAD HOLLOW0002 MAX
 DEBURR EDGES OF GEAR TEETH015 MAX

REFERENCE DATA

PITCH DIAMETER 2.06621
 BASE CIRCLE DIAMETER 1.96073
 BASE PITCH11623
 MEASUREMENT OVER TWO .068 DIAMETER PINS 2.1874 12.1851
 CENTER DISTANCE, OPERATING 1.3750
 BACKLASH, OPERATING0035 1.0018
 DESIGNED TO MATE WITH PART NUMBER 16TSUN 122T RING

Ring Gear - 1

Feb 01 03 08:47p GEORGE BOWERS 765 349 9828 p.6

GEAR TECHNOLOGY APPLIED, INC.
3540 WOODLAND POINT
MARTINSVILLE, IN 46151-8087

PART NUMBER P-1 & P-2
 PART NAME RING GEAR 122T ORIGINATOR G.L. BOWERS
 MODEL PLANETARY TRANSMISSION
 DATE 1-29-2003 APPROVAL LB

INTERNAL INVOLUTE SPUR GEAR DATA

NUMBER OF TEETH 122
 DIAMETRAL PITCH (MODULE (METRIC MOD.)) 25.4
 PRESSURE ANGLE 20°
 INSIDE DIAMETER 4.798 14.794
 TIP CHAMFER DIAMETER 4.798 MAX
 ACTIVE PROFILE DIAMETER 4.913
 ROOT DIAMETER 4.941 14.936
 ROOT FILLET RADIUS FULL020 MIN
 CIRCULAR TOOTH THICKNESS0448 1.0440
 LEAD TOLERANCE ACROSS $B_0/2$ FACE WIDTH LESS BREAK
 MINUS MATERIAL ONLY / OUTSIDE $B_0/2$ BOTH SIDES +0.0004 1 - 0.004 AVG
 LEAD VARIATION0006 MAX
 LEAD CROWN0002 MAX
 LEAD HOLLOW0002 MAX
 DEBURR EDGES OF GEAR TEETH015 MAX

REFERENCE DATA

PITCH DIAMETER 4.80315
 BASE CIRCLE DIAMETER 4.51343
 BASE PITCH11623
 MEASUREMENT BETWEEN TWO .068 DIAMETER PINS 4.7528 14.7550
 CENTER DISTANCE, OPERATING 1.3750
 BACKLASH, OPERATING0035 1 - 0.018
 DESIGNED TO MATE WITH PART NUMBER 53T (PLANET-PIGION)

Sun Gear - 2

Feb 01 03 08:47p GEORGE BOWERS 765 349 9828 p.8

GEAR TECHNOLOGY APPLIED, INC.
3540 WOODLAND POINT
MARTINSVILLE, IN 46151-8087

PART NUMBER P-3
PART NAME SUN ROT ORIGINATOR G.L. BOWERS
MODEL PLANETARY TRANSMISSION
DATE 1-29-2007 APPROVAL LBG

EXTERNAL INVOLUTE SPUR GEAR DATA

NUMBER OF TEETH 20
DIAMETRAL PITCH / MODULE (METRIC MOD.) 25.4
PRESSURE ANGLE 20°
OUTSIDE DIAMETER875 / .871
TIP CHAMFER DIAMETER871 MIN
ACTIVE PROFILE DIAMETER753
ROOT DIAMETER699 / .694
ROOT FILLET RADIUS FULL019 MIN
CIRCULAR TOOTH THICKNESS0644 / 1.0636
LEAD TOLERANCE ACROSS 80% FACE WIDTH LESS BOTH SIDES + .0003 / - .0003 AVG
END EDGE CHAM/BREAK
MINUS MATERIAL ONLY OUTSIDE THE 80%
LEAD VARIATION0002 MAX
LEAD CROWN0002 MAX
LEAD HOLLOW0002 MAX
DEBURR EDGES OF GEAR TEETH015 MAX

REFERENCE DATA

PITCH DIAMETER78740
BASE CIRCLE DIAMETER73992
BASE PITCH11623
MEASUREMENT OVER TWO .068 DIAMETER PINS8871 / .8853
CENTER DISTANCE, OPERATING 1.375
BACKLASH, OPERATING0035 / .0018
DESIGNED TO MATE WITH PART NUMBER 50 T PLANE - PINION

Planet Gear - 2

Feb 01 03 08:47p

GEORGE BOWERS

765 349 9828

p.10

GEAR TECHNOLOGY APPLIED, INC.
3540 WOODLAND POINT
MARTINSVILLE, IN 46151-8087

PART NUMBER P-3
 PART NAME PLANET PINION 5DT ORIGINATOR G.L. BOWERS
 MODEL PLANETARY TRANSMISSION
 DATE 1-29-2003 APPROVAL [Signature]

EXTERNAL INVOLUTE SPUR GEAR DATA

NUMBER OF TEETH 50
 DIAMETRAL PITCH P (MODULE M METRIC MOD.) 25.4
 PRESSURE ANGLE 20°
 OUTSIDE DIAMETER 2.010 12.006
 TIP CHAMFER DIAMETER 2.006 MIN
 ACTIVE PROFILE DIAMETER 1.906
 ROOT DIAMETER 1.855 1.950
 ROOT FILLET RADIUS FULL019 MIN
 CIRCULAR TOOTH THICKNESS0553 1.0545
 LEAD TOLERANCE ACROSS BOTH FACE WIDTH LESS
EDGE OF CHE/BREAK BOTH SIDES + .0003 - .0023 AVG
MINUS MATERIAL ONLY OUTSIDE BOTH
 LEAD VARIATION0005 MAX
 LEAD CROWN0004 MAX.
 LEAD HOLLOW0002 MAX
 DEBURR EDGES OF GEAR TEETH015 MAX

REFERENCE DATA

PITCH DIAMETER 1.96850
 BASE CIRCLE DIAMETER 1.84977
 BASE PITCH11623
 MEASUREMENT OVER TWO .063 DIAMETER PINS 2.0472 12.0451
 CENTER DISTANCE, OPERATING 1.3750
 BACKLASH, OPERATING0035 1.0218
 DESIGNED TO MATE WITH PART NUMBER 20TSUN & 12L TRING

Ring Gear - 2

Feb 01 03 08:48p

GEORGE BOWERS

765 349 9828

p.12

GEAR TECHNOLOGY APPLIED, INC.
3540 WOODLAND POINT
MARTINSVILLE, IN 46151-8087

PART NUMBER P23
PART NAME RING GEAR 121T ORIGINATOR G.L. BOWERS
MODEL PLANETARY TRANSMISSION
DATE 1-29-2003 APPROVAL LB

INTERNAL INVOLUTE SPUR GEAR DATA

NUMBER OF TEETH	<u>121</u>
DIAMETRAL PITCH / MODULE (<u>4 METRIC MOD.</u>)	<u>25.4</u>
PRESSURE ANGLE	<u>20°</u>
INSIDE DIAMETER	<u>4.658</u> <u>1.4.654</u>
TIP CHAMFER DIAMETER	<u>4.658</u> MAX
ACTIVE PROFILE DIAMETER	<u>4.754</u>
ROOT DIAMETER	<u>4.805</u> <u>-1.800</u>
ROOT FILLET RADIUS <u>FULL</u>	<u>.020</u> MIN
CIRCULAR TOOTH THICKNESS	<u>.0819</u> <u>1.0811</u>
LEAD TOLERANCE ACROSS <u>80%</u> FACE WIDTH <u>LESS</u> <u>END EDGE CHF. / BREAK</u> BOTH SIDES	<u>+ .0004</u> <u>- .0004</u> AVG
<u>MINUS MATERIAL ONLY OUTSIDE 80%</u> LEAD VARIATION	<u>.0006</u> MAX
LEAD CROWN	<u>.0002</u>
LEAD HOLLOW	<u>.0002</u> MAX
DEBURR EDGES OF GEAR TEETH	<u>.015</u> MAX

REFERENCE DATA

PITCH DIAMETER	<u>4.763713</u>
BASE CIRCLE DIAMETER	<u>4.47642</u>
BASE PITCH	<u>.11623</u>
MEASUREMENT BETWEEN TWO <u>.068</u> DIAMETER PINS	<u>4.6043</u> <u>1.4.6069</u>
CENTER DISTANCE, OPERATING	<u>1.3750</u>
BACKLASH, OPERATING	<u>.0035</u> <u>1.0018</u>
DESIGNED TO MATE WITH PART NUMBER	<u>PLANET PINION 50T</u>

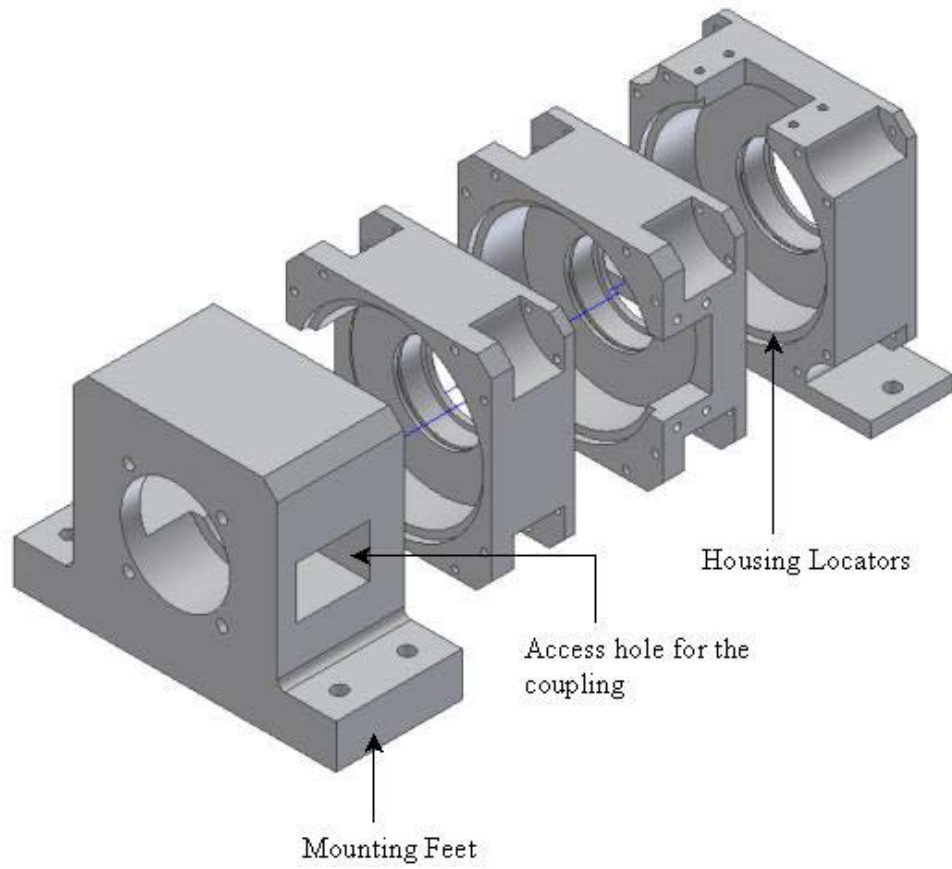
Non-Standard Gears

Non-standard gears are used in the DVT to fit a predetermined center distance value and to obtain the ratios required, as mentioned before. With a non-standard gear, the standard tooth proportions are not satisfied. In other words, the meshing gears do not have same addendum, dedendum or tooth thickness. Also the center distance is not the average of the pitch diameters. Let us consider the following table to show the DVT gears are non-standard. As an example, sun and planet gears of the first and second stage planetary are considered. It can be seen that the tooth proportions do not agree with the AGMA standards. The diametral pitch (P) in the current design is 25.4.

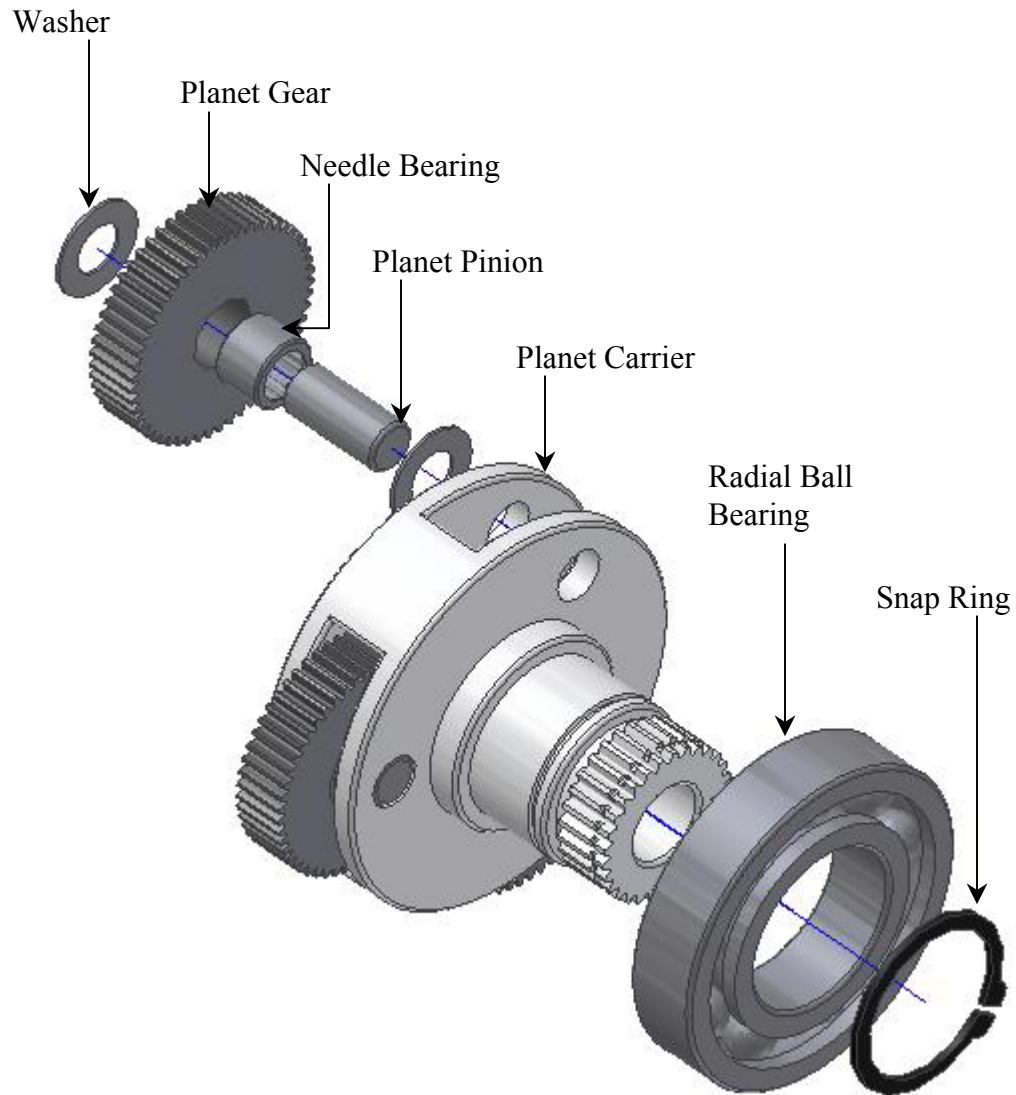
Table A1 – Comparison between Standard and Non-standard gears

Symbol	Definition	AGMA Standard	Current Design	
			Sun Gear - 1	Planet Gear - 1
ϕ	Pressure Angle	20°	20°	20°
a	Addendum	1.000/ P	0.102	0.079
b	Dedendum	1.250/ P	0.072	0.088
t	Tooth Thickness	$\Pi/2P$	0.0703	0.0643
N'_P	Min. number of teeth Pinion Gear	18 36	16	53

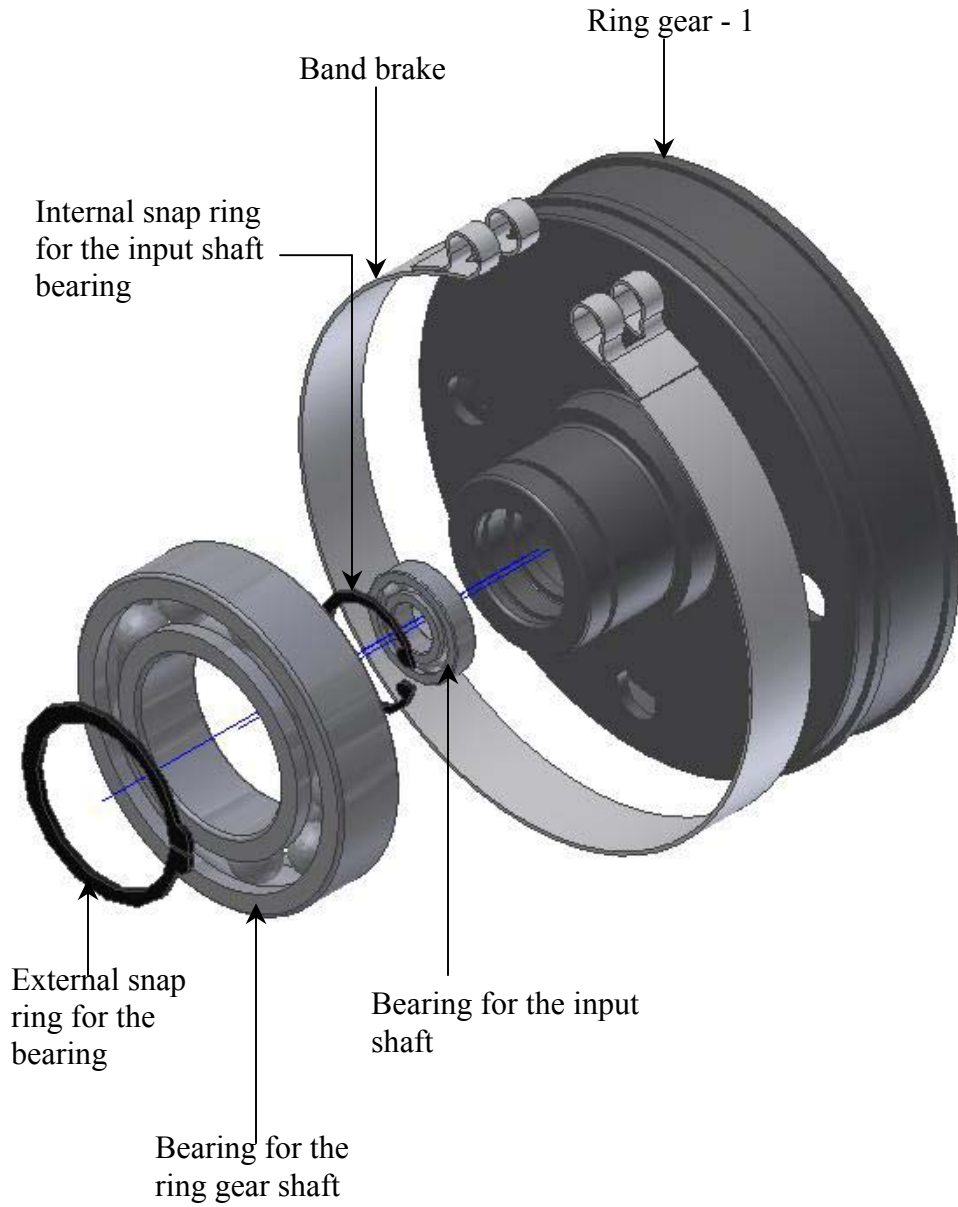
Exploded view of the DVT Housing



Exploded view of the Carrier Assembly



Exploded view of the Ring Gear assembly



Detailed Drawings Of DVT Components

1. Input Shaft with the Sun Gears	Sun_InputShaft.pdf
2. Planet Gear –1	MDPlanet1_2.pdf
3. Planet Gear – 2	MDPlanet3.pdf
4. Ring Gear –1	MDRing1.pdf
5. Ring Gear – 2	MDRing2.pdf
6. Ring Gear – 3	MDRing3.pdf
7. Carriers – 1&2	MDCarrier1-2.pdf
8. Carrier – 3	MDCarrier3.pdf
9. Housing 1	House1.pdf
10. Housing 2	House2.pdf
11. Housing 3	House3.pdf
12. Housing 4	House4.pdf
13. Planet Pins	Carrierpin.pdf
14. Band Brake	Bandbrake.pdf
15. Link connecting band brake and yoke	BandtoYokeLink.pdf
16. Yoke Piece	New_Yoke1.pdf
17. Link connecting yoke and crank	New_link4.pdf
18. Crank	Crank.pdf
19. L-Bracket	New_Bracketcv.pdf
20. Spacer	Spacer.pdf
21. Yoke Pins	Yoke_Pins.pdf

- | | |
|------------------------------|--------------------------------|
| 22. Band Pins | Brake_Pin.pdf |
| 23. Crank Pin | Crank_Pin.pdf |
| 24. Final DVT 3D model | 3DFinalDVT.pdf |
| 25. Cross Section of the DVT | FinalDVT.pdf |

Ratio Calculations For A Two-Stage DVT

For the two-stage DVT let us consider the same gears that are used in the current design and estimate the amount of reductions possible. Refer to Figure 36 along with this discussion. The gear data is:

First stage planetary

Number of sun gear teeth – 20

Number of planet gear teeth – 50

Number of ring gear teeth – 121

Second stage planetary

Number of sun gear teeth – 16

Number of planet gear teeth – 53

Number of ring gear teeth – 122

Gear 1

Brake B1 is engaged. The configuration is carrier-ring. For an input speed of 5000rpm, the carrier output speed is given by equation 3.1. Hence the output speed is 579.71rpm, which is reduction of around 9:1.

Gear 2

Brake B2 is engaged and the clutch mechanism diverts the power flow so that the configuration becomes a carrier-carrier. Hence the carrier speeds are the same. A gear reduction takes place in the first stage, which is the output speed of 709.219rpm. This gives a reduction in the order of 7:1.

Gear 3

Brake B2 is engaged and the configuration is carrier-ring. Again, for an input speed of 5000rpm, the final carrier output is calculated as 1206.7rpm. This gives a reduction of approximately 4:1.

So this configuration gives an output speed range of 4 – 9 rpm in two stages, which is really encouraging. The output speeds of this system are lesser than that of the current design, which also reduces the weight of the final reduction. This system combined with a reduction of 150:1 can provide arm speeds in the range of 4 – 8rpm. Control issues related with the gear shifting in this configuration are important things to look at.

VITA

Sriram Sridharan was born in Kottaiyur, Tamil Nadu, India on the 21ST day of February 1979. He was brought up at the south Indian city of Chennai where he was educated. He obtained his bachelors degree in mechanical engineering from the University of Madras, Chennai in July 2000. A year later he decided to further his education in the United States of America when he came to the University of Tennessee, Knoxville. He was awarded a masters degree in mechanical engineering in spring of 2004.